# Speciation and distribution of chromium (III) in rice root tip and mature zone: The significant impact of root exudation and iron plaque on chromium bioavailability

Peiman Zandi, Xing Xia, Jianjun Yang, Jin Liu, Laurent Remusat, Cornelia Rumpel, Elke Bloem, Beata Barabasz Krasny, Ewald Schnug

Journal of Hazardous Materials

# Speciation and distribution of chromium (Cr) in rice root tip and mature zone: the importance and impact of root exudation and iron plaque in Cr bioavailability

--Manuscript Draft--

| | |
|---|---|
| **Manuscript Number:** | HAZMAT-D-22-13168R1 |
| **Article Type:** | Research Paper |
| **Keywords:** | Cr-speciation; Iron-plaque dissolution; NanoSIMS analysis; phytometabolites; root morphology |
| **Corresponding Author:** | Jianjun Yang, Prof. PhD.<br>Chinese Academy of Agricultural Sciences Institute of Environment and Sustainable Development in Agriculture<br>Beijing, CHINA |
| **First Author:** | Peiman Zandi, Assistant Prof. |
| **Order of Authors:** | Peiman Zandi, Assistant Prof. |
| | Xing Xia, PhD |
| | Jianjun Yang, Prof. PhD. |
| | Jin Liu, Associate Prof. |
| | Remusat Laurent, PhD |
| | Cornelia Rumpel, Prof. |
| | Elke Bloem, PhD |
| | Beata Barabasz Krasny, Associate Prof. |
| | Ewald Schnug, Prof. Dr |
| **Suggested Reviewers:** | Hamid Madani, PhD<br>Prof., Islamic Azad University Arak Branch<br>h-madani@iau-arak.ac.ir |
| | Ameer Hussain Jarwar, PhD<br>Agricultural Research Institute<br>jhomper@gmail.com |
| | Donald Spark, PhD<br>Prof., University of Delaware<br>dlsparks@udel.edu |

Graphical Abstract

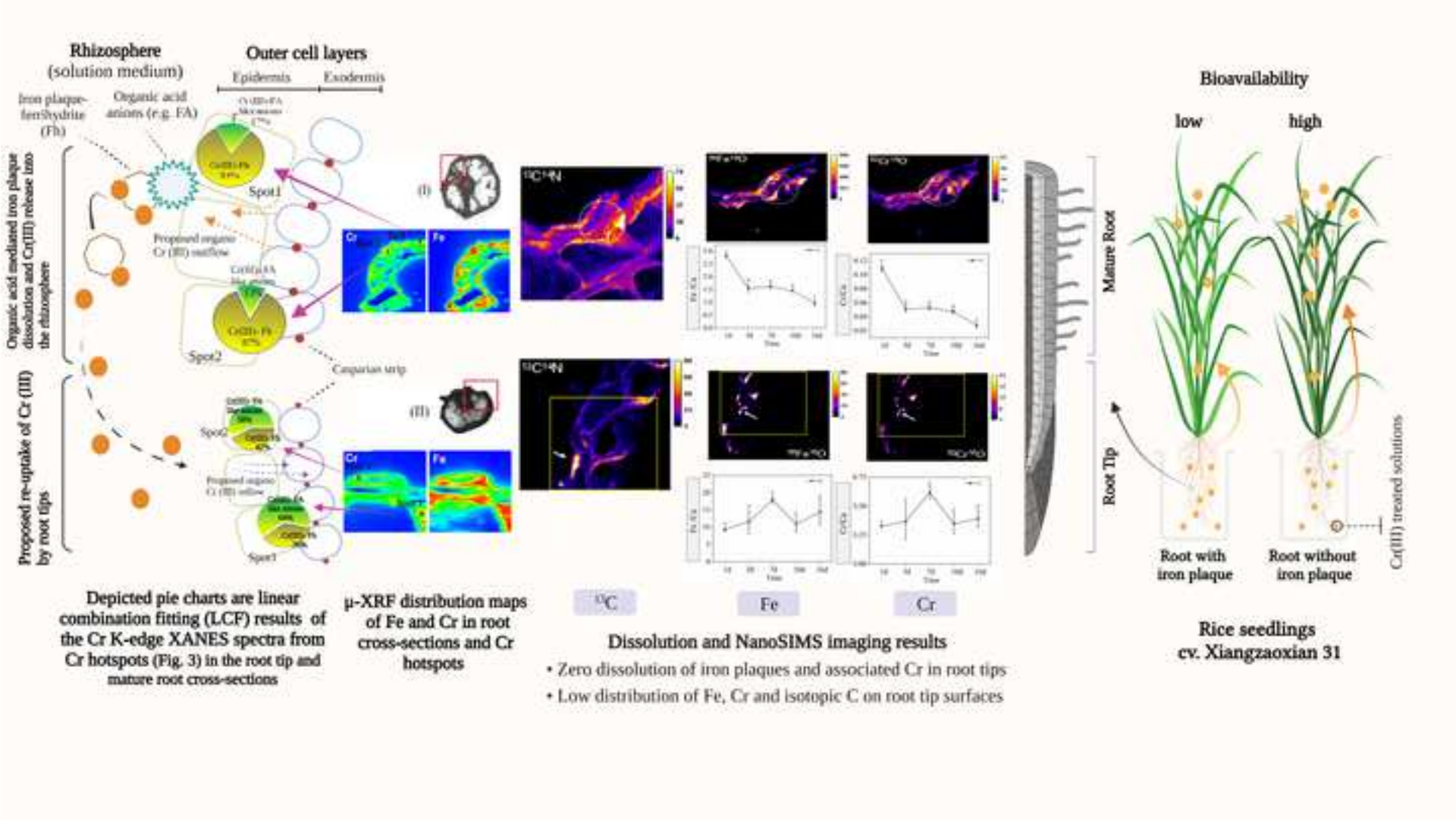

# Speciation and distribution of chromium (Cr) in rice root tip and mature zone: the importance and impact of root exudation and iron plaque in Cr bioavailability

**Peiman Zandi[a#,b], Xing Xia[a#], Jianjun Yang[a*], Jin Liu[c], Remusat Laurent[d], Cornelia Rumpel[e], Elke Bloem[f], Beata Barabasz Krasny[g], Ewald Schnug[h]**

[a] Institute of Environment and Sustainable Development in Agriculture, Chinese Academy of Agricultural Science, Beijing 100081, P. R. China

[b] International Faculty of Applied Technology, Yibin University, Yibin 644000, China

[c] College of Agronomy and Biotechnology, China Agricultural University, Beijing 100094, China

[d] Muséum National d'Histoire Naturelle, Institut de Minéralogie, Physique des Matériaux et Cosmochimie, CNRS UMR 7590, Sorbonne Université, 75005 Paris, France

[e] CNRS, Institute of Ecology and Environmental Sciences of Paris, IEES, UMR (CNRS-INRA-UPMC-UPEC-IRD), Thiverval-Grignon, 78850, France

[f] Julius Kühn-Institut, Federal Research Centre for Cultivated Plants, Institute for Crop and Soil Sciences, Bundesallee 69, 38116 Braunschweig, Germany

[g] Institute of Biology, Pedagogical University of Krakow, Podchorążych 2 St., 30-084 Kraków, Poland

[h] Institute for Plant Biology, Department of Life Sciences, Technical University of Braunschweig, 38106 Braunschweig, Germany

[#]Xing Xia and Peiman Zandi equally contributed to this work.

* Corresponding author.

E-mail address: yangjianjun@caas.cn; yangjianjun-caas@outlook.com (J. Yang)

# Speciation and distribution of chromium (Cr) in rice root tip and mature zone: the importance and impact of root exudation and iron plaque in Cr bioavailability


## Abstract

Evidence on the contribution of root regions with varied maturity levels in iron plaque (IP) formation and root exudation of metabolites and their consequences for uptake and bioavailability of chromium (Cr) remains unknown. Therefore, we applied combined nanoscale secondary ion mass spectrometry (NanoSIMS) and synchrotron-based techniques, micro-X-ray fluorescence (μ-XRF) and micro-X-ray absorption near-edge structure (μ-XANES) to examine the speciation and localisation of Cr and the distribution of (micro-) nutrients in rice root tip and mature region. μ-XRF mapping revealed that the distribution of Cr and (micro-) nutrients varied between root regions. Cr K-edge XANES analysis at Cr hotspots attributed the dominant speciation of Cr in outer (epidermal and sub-epidermal) cell layers of the root tips and mature root to Cr(III)-FA (fulvic acid-like anions) (58-64%) and Cr(III)-Fh (amorphous ferrihydrite) (83-87%) complexes, respectively. The co-occurrence of a high proportion of Cr(III)-FA species and strong co-location signals of $^{52}Cr^{16}O$ and $^{13}C^{14}N$ in the mature root epidermis relative to the sub-epidermis indicated an association of Cr with active root surfaces, where the dissolution of IP and release of their associated Cr are likely subject to the mediation of organic anions. The results of NanoSIMS (poor $^{52}Cr^{16}O$ and $^{13}C^{14}N$ signals), dissolution (no IP dissolution) and μ-XANES (64% in sub-epidermis >58% in the epidermis for Cr(III)-FA species) analyses of root tips may be indicative of the possible re-uptake of Cr by this region. The results of this research work highlight the significance of IP and organic anions in rice root systems on the bioavailability and dynamics of Cr.



**Keywords:** Cr-speciation, Iron-plaque dissolution, NanoSIMS analysis, phytometabolites, root morphology


## Environmental Implications

Considering how different root regions with varied iron plaque presence, dissolution rate, and diverse root metabolites and their exudations may affect the fate of Cr uptake and bioavailability in rice plants, the present study has, for the first time, set the stage for holistic investigation of two critical parts of the root (tip/mature root) system at a molecular level using combined NanoSIMS and synchrotron-based (μ-XRF/ μ-XANES) techniques. The findings of this study appear to be significant for current and future studies on suppressing heavy metal bioavailability in contaminated paddy soil systems.

## 1. Introduction

Soil contamination with heavy metals, especially chromium (Cr), is a widespread problem that poses threats to human health risks through the food chain (Yang et al., 2019a; Ali et al., 2022). In China, Cr is one of the eight heavy metals most strongly affecting agricultural soils, with a contamination rate exceeding 1.1% (Zhao et al., 2015). Based on the China National Food Hygiene Standard (GB 2762-2017), the bioaccessibility of Cr in rice grain should not exceed the Cr threshold value of 1.0 $mg{\cdot}kg^{-1}$ (Geng et al., 2020; Ali et al., 2022) to avoid adverse health complications (e.g., oxidative stress and DNA damage) associated with dietary Cr intake (Nickens et al., 2010; Khan et al., 2012). Therefore, controlling Cr transfer in the soil-rice system is crucial for food safety.

Root uptake in rice is considered to be the major entry route of soil Cr into edible rice grains. The root system of rice plants consists of seminal, nodal (primary), and lateral roots (Gu et al., 2017). Among them, primary roots are classified into root tips and mature root regions according to the level of development (Seyferth et al., 2010; Zandi et al., 2022). Root tips have underdeveloped vascular systems, lacking the complete formation of the aerenchyma and Casparian bands (CBs). They account only for a small fraction of the overall mineral element uptake in rice plants, while mature rice roots have a fully developed anatomical structure with the cortex (exodermis, aerenchyma, endodermis) and stele (xylem) that support the influx and transport of mineral nutrients (Yamaji and Ma, 2007; Coudert et al., 2010; Fukao et al., 2019).

Similarly to many aquatic or semi-aquatic plants, rice is a hydrophyte species grown in flooded paddy fields. Rice has to cope with anaerobic conditions by radial oxygen diffusion from the root aerenchyma towards the root surface and adjacent rhizosphere (Deng et al., 2010; Xu et al., 2018), where it mediates iron oxidation [Fe (II) to Fe (III)] and development of an amorphous coating of iron (hydr)oxides (known as iron plaque, IP) on the root surface (Cheng et al., 2014; Tripathi et al., 2014; Zandi et al., 2022). Moreover, continuous flooding was indicated to create a favourable rhizosphere environment for IP formation (Xiao et al., 2021). The physical barrier of IP has been proposed to serve as a natural protection mechanism against excess heavy metal concentration in plant parts (Khan et al., 2016).

There is consensus that root capacity for aerobic respiration is the main factor in the oxidising power of the rhizoplane zone (Wu et al., 2012; Holzschuh et al., 2014), and consequently the degree of IP formation (Zandi et al., 2022). Rice root tips with no discernible aerenchyma structures were found to have a higher oxygen discharge in comparison to the basal part of the root (Nishiuchi et al., 2012). Nonetheless, IP was shown to be less frequent around the root tips (Williams et al., 2014) due to their rapid development (Nishiuchi et al., 2012), possibly affecting heavy metal speciation and mobility in this region compared to the basal root region.

Many studies concerning the whole root system have shown that iron (hydr)oxides have a strong binding affinity for metal(loid) ions on the root surface and reduce their mobility and bioavailability, thereby inhibiting the uptake and transport of toxic metals, including Cr (Hu et al., 2014; Cao et al., 2018; Zandi et al., 2022). Previous studies have shown that in the absence or weak presence of IP, higher concentrations of Cr were accumulated in root cells rather than in shoots of rice (Xu et al., 2018; Zandi et al., 2020, 2021), suggesting that Cr mainly deposited in root cell walls hindered its transport to the aerial organs (Zeng et al., 2011). The hydroponic and soil culture experiments have demonstrated that an appropriate amount of IP on root surfaces could effectively adsorb Cr(III) and Cr(VI) species and reduce their transfer to the rice roots and shoots, thus decreasing Cr concentrations in rice tissues (Xu et al., 2018; Yu et al., 2017; Zandi et al., 2020).

In addition to the inhibition of iron (hydr)oxides, other factors such as root exudates, which mainly consist of low or fairly low molecular weight (LMW) organic anion metabolites, with various

chemical functional groups (e.g., –COOH, –OH) (Seal et al., 2004), have been proposed to interact with iron (hydr)oxides during sorption and chelation of heavy metals in the soil (Zhang et al., 2020) and plant systems (Wang et al., 2019). Moreover, earlier studies have shown that these metabolites can enhance the dissolution of iron (hydr)oxides bound to heavy metals, leading to their release into the rhizosphere (Sebastian and Prasad, 2016; Luo et al., 2017; Saad et al., 2017). Studies on the entire root system in environments contaminated with cadmium (Cd), aluminium (Al) and Cr have indicated that organic anion secretions are highly associated with increased heavy metal tolerance through their efflux into the rhizosphere (Yang et al., 2013; Saad et al., 2017; Yang et al., 2019b; Bali et al., 2020). This efficient exclusion mechanism reduces metal uptake and accumulation in plants (Montiel-Rozas et al., 2016).

In the rice root system, these metabolites may also act as a defensive barrier for the roots by forming stable complexes with Cr (Uren, 2000; Zeng et al., 2008) or affecting their reduction and immobilisation in the root (Xiao et al., 2023). Therefore, the contribution of root exudates to increased Cr accumulation in rice roots could be related to the tolerance mechanism through chelation (Hayat et al., 2012; Agnello et al., 2014). The rate and composition of metabolites released in response to Cr stress correlate with plant genotype (Zeng et al., 2008) and metal speciation of Cr (Pradas del Real et al., 2014).

Previous studies on the importance of IP or root exudation in suppressing the bioavailability of heavy metal Cr in rice plants mainly focused on the evaluation of the entire root system (Zandi et al., 2020; Xiao et al., 2023). This study has addressed for the first time how individual root regions with varied maturity levels (e.g., less developed tips) may differ in the degree of IP formation or in the secretion of organic anions in response to Cr stress. Further, the issues concerning the correlation of these secretions with IP dissolution and Cr release, and whether IP dissolution mediated by root metabolites can alter Cr mobility and bioavailability have also been analysed. Moreover, it remains unclear whether the main root regions vary in their contribution to Cr chelation and immobilisation, and reduced Cr accumulation in tissues under the influence of iron plaque and root exudation.

To bridge the gap, the present study explicitly proposed the combined application of state-of-the-art high-sensitivity ion mass spectrometry (NanoSIMS) and synchrotron-based microprobe techniques,

such as micro-X-ray absorption near-edge structure spectroscopy (μ-XANES) and micro-beam X-ray fluorescence (μ–XRF), to investigate the distribution and/or speciation of elements of interest (X) in different root regions (root tips/ mature root) of rice at submicro- and microspatial scales, and their association with $^{13}C$-labelled root exudates on the active root surface.

The objectives of this study were to (1) explain/assess the interaction between Cr and Fe and its effect on Cr uptake and translocation in rice plants, (2) elucidate the molecular speciation of Cr and binding mechanisms of Cr species in different root regions, and (3) to localise the active root surface with exudate release and its impact on Cr uptake by different root regions. We expected that these results would provide a theoretical basis for understanding heavy metal sequestration and dynamics on iron plaques and their benefits to human health by reducing rice contamination. We expected that these results would provide a theoretical basis for understanding heavy metal sequestration and dynamics on iron plaques and their benefit to human health by reducing rice contamination.

## 2. Materials and methods

### 2.1. Plant culture, treatments and metal extraction

Rice seed (*Oryza sativa* L. Var. Xiangzaoxian 31) germination (7 days on moist gauze in plastic Petri dishes in the dark at 28°C) and initial growth (21 days in black plastic containers) were conducted under controlled sterile conditions in half-strength nutrient solution (Table Supplementary (S) 1-S1), as previously described (Zandi et al., 2021). The variety was a high-quality, early-maturing, hybrid-based (Chen et al., 2000; Yu, 2018) model crop for bioremediation studies used at the Institute of Environment and Sustainable Development in Agriculture, Chinese Academy of Agricultural Sciences in Beijing.

The seedlings of the first group, intended for iron plaque (IP) formation (Fe80-CK; Fig. S1), were transferred to solutions spiked with 80 mg $L^{-1}$ ferrous iron ($FeSO_4 \cdot 7H_2O$), incubated for 24 h and subsequently transferred into quarter strength and total strength nutrient solution for 2 and 3 days, respectively. The second group (Fe0-Cr(III)) was not subjected to IP induction, but was grown in a nutrient solution containing 1.0 mg $L^{-1}$ $CrCl_3 \cdot 6H_2O$ for 3 days, and then transferred to a quarter-

strength nutrient solution for 2 days. The first two groups were exclusively designed for bioavailability analysis and were not included in the follow-up investigations described in sections 2.2, 2.3 and 2.4. The third group (Fe80-Cr(III)) was a combination of the two aforementioned treatments, where seedlings with IP were exposed to Cr(III)-spiked solutions for 3 days. Each treatment was performed in three replicates. Replenishment of depleted nutrients in culture solutions was carried out every three days, and manual adjustment of the solutions to a suitable pH of 5.5 was done using 0.1 M HCl and NaOH (Zandi et al., 2020). All seedlings were grown in a controlled plant growth chamber (PGX-350D, NSEI Co., Ltd., China) with a relative humidity of 70% dedicated to predetermined periodic dark (10 h, 20 °C ) and light (14 h, 28 °C, 300-350 µmol $m^{-2}s^{-1}$) regimes. The selected Fe and Cr concentrations were based on recommendations and results of earlier studies (Hu e al. 2014; Li et al., 2015; Yu et al., 2017; Zandi et al., 2020).

The seedlings were collected, split into roots and shoots and rinsed with deionised water. Fresh roots with IP were initially divided into the tip (from the root cap to the zone without root hair; ~2-3 cm) and mature (from the root hair zone to the base of primary roots) sections, and subsequently incubated for 30 min at room temperature (25°C) in 30 mL of cold DCB (dithionite–citrate–bicarbonate) solution containing $NaHCO_3$ (0.125 M), $Na_3C_6H_5O_7$ (0.03 M) and $Na_2S_2O_4$ (0.5 g) (Liu et al., 2004). After incubation, the sections were thoroughly washed with deionised water and removed from incubation tubes. The remaining extracts were initially filled up with deionised water to a volume of 50 mL and subsequently passed through a 0.45-µm filter to remove root debris.

The digestion of plant materials was carried out according to Hu et al. (2014) with some modifications. Briefly, plaque-free root sections were oven-dried (similar to shoot samples) and homogenised, pre-digested overnight in heat-proof tubes (100 mL) in 5 mL of concentrated $HNO_3$ (~65-68%). Digestion was completed in a digester heating block at 160°C for ~3 h and after cooling to room temperature, diluted in 25 mL of deionised water and filtered. A reagent blank and a series of external standard solutions (e.g., GBW07605) from certified reference materials in China were utilised to validate the quality control and accuracy of the entire digestion procedure. Fe and Cr contents in the digestion solutions and DCB extracts were quantified using ICP-OES (Agilent 5110, Agilent Technologies, Inc., USA).

## 2.2. Synchrotron-based microprobe analysis

Freshly sectioned root specimens were stored at –30°C until synchrotron-based microprobe analyses. For μ-XRF imaging of root surfaces using the VESPERS beamline at the Canadian Light Source (CLS), the roots were sectioned and flatly fixed on a Kapton tape. For μ-XRF/μ-XANES analyses of root cross sections using the 15U beamline at the Shanghai Synchrotron Radiation Facility (SSRF, Shanghai), the corresponding root sections were cut into 60-μm-thick slices by a microtome, and subsequently mounted onto a Kapton tape for freeze-drying and stored at –20°C (Tian et al., 2010; Lu et al., 2017). As described in previous studies (Yang et al., 2015; Wang et al., 2021), the μ-XRF method of both beamlines was similar, except that the data in VESPERS were analysed using SMRK software, thus here we have only reported the experimental details for the 15U beamline at the SSRF.

X-rays with an incident energy of 10 keV were monochromatised using a Si (111) double-crystal monochromator. The spot size of the X-ray beam was micro-focused to 10 μm x 5 μm using a Kirkpatrick-Baez (K-B) mirror system for scanning. The root samples were placed at an angle of 45° to the beam incidence perpendicular to a 7-element Si(Li) detector (e2v, USA). After selecting the region of interest by the microscope, the region was scanned step by step by moving the sample stage with a step size of 5 and 10 μm for x and y direction, respectively. First, the whole fluorescence spectrum was acquired, and then the fluorescence signals of the elements of interest, including K (3.3 keV), Ca (3.6 keV), Cr (5.4 keV), Mn (5.9 keV), Fe (6.4 keV) were selected and applied to all pixel spectra to obtain multi-elemental 2D mapping with a dwell time of 1.5 s per pixel. After analysing the μ-XRF images using Igor Pro 6.0 software (IGOR), the spots of interest were selected for Cr K-edge μ-XANES spectra collection in the fluorescence mode at 25°C. The energy range and step were set to 5931-6080 eV and 0.5 eV, respectively. Several scans were collected from each spot and later averaged to obtain a merged spectrum with a better signal-to-noise ratio. At least 2 hotspots from cross-sections of the root tips and mature root regions were considered for μ-XANES spectrum collection. Cr foil was also used to calibrate the beamline (X-ray) energy.

Cr K edge μ-XANES spectra of Cr(III) adsorbed on ferrihydrite (Cr(III)-Fh) and organo-Cr(III) complexes (Cr(III)-FA) (synthesised by the interaction of $CrCl_3$ with fulvic acid) (Yang et al., 2020) were acquired in the fluorescence mode and Cr(III) acetate in the total electron yield mode, and were

192 referred to as Cr reference standards. Since root iron plaques induced in a short 24-h period were
193 poorly crystallised and mostly amorphous (Xu and Yu, 2013), ferrihydrite, a typical amorphous iron
194 (hydr)oxide formed during iron hydrolysis (Yang et al., 2020), was considered as the principal sorbent
195 for Cr (III) sequestration in rice root IP in this study. Athena software (Ver. 2.1.1) was used for
196 fingerprint and linear combination fitting (LCF) analysis of sample μ-XANES spectra (Ravel and
197 Newville, 2005). Cr speciation and the percentage of each Cr species were determined based on the
198 LCF of Cr K-edge μ-XANES spectra of the hotspots using the spectra of the reference compounds as
199 end-members (Peng et al., 2015). The goodness of data fitting was assessed using the R-factor.
200 It should be noted that the limited root samples (one sample/ root section) and spots (2 hotspots/
201 root cross-sections) measured during the μ-XRF and μ-XANES analyses may not be representative of
202 the whole root samples. However, earlier studies used a similar method and have demonstrated that
203 the output result could account for most of the sample variation (Lombi and Susini, 2009; Seyfferth et
204 al., 2010; Frommer et al., 2011; Li et al., 2015; Yang et al., 2015).
205
206 2.3. $^{13}CO_2$ labelling of rice and NanoSIMS analysis
207 The procedure for uniform $^{13}CO_2$ labelling of rice was as described earlier (Ge et al., 2012; Yuan et al.,
208 2016) with some modifications. Briefly, rice seedlings belonging to the third treatment group (Fe80-
209 Cr (III)) were first exposed to $CrCl_3$ treatment for 24 h and subsequently transferred to normal (Cr-
210 free) nutrient solution and kept in transparent airtight perspex $^{13}CO_2$-labelling and non-labelling
211 control boxes (40 cm long × 50 cm wide × 60 cm high; Fig. S2) for 24 h. During this period, the
212 concentration of $^{13}CO_2$ inside the labelling box atmosphere was maintained at approximately
213 400 μL $L^{-1}$ (ppm) by controlled injection of 0.1 M $Na_2{}^{13}CO_3$ solution ($^{13}$C-enriched > 99%) into 1 M
214 HCl solution. A $CO_2$ detector spectrometer (IRMS, RS-CO2WS-N01-2, Shandong Renke Control
215 Technol. Co., Ltd., China) was used to monitor $CO_2$ concentration inside the labelling boxes (Kaiser
216 et al., 2015). Isotopic labelling of rice seedlings with $^{13}$C was performed by photosynthetic fixation of
217 $^{13}CO_2$ in the aforementioned labelling boxes. Seedlings incubated in unlabelled control boxes served
218 as the reference factor for excess $^{13}$C in shoots and roots after DCB extraction. The environmental
219 growth conditions in the perspex boxes were identical to those described in section 2.1.

Rice seedlings were harvested and separated into roots and shoots before IP dissolution could occur, e.g., as a result of the secretion of $^{13}C$-labelled and/or unlabelled metabolites by the roots. Afterwards, root and shoot samples from both labelled and unlabelled control seedlings were ground to determine $^{13}C$ abundance in the respective plant samples using a C/N element analyser coupled to an isotope ratio mass spectrometer to verify successful labelling with $^{13}C$ (Isoprime 100, Elementar's PYE cube, UK). Freshly sectioned root specimens were immersed in a tissue freezing medium (SAKURA Tissue-Tek OCT) for rapid freezing at −30°C. Root sections were then axially frozen-cut into 60-µm-thick slices using a microtome (Reichert-Jung, Germany). The slices were collected and mounted onto a $Si_3N_4$ wafer and coated with gold (20 nm thick) for NanoSIMS analysis.

Cross-sections of mature roots and root tips were imaged using Cameca NanoSIMS 50 installed at the Museum National d'Histoire Naturelle, Paris, France. The surfaces of the root samples were scanned with a 16 keV $Cs^+$ (caesium) primary beam, set to 1 pA, leading to a spatial resolution of approximately 150 nm. Secondary ions were collected in multicollection mode: $^{12}C^-$, $^{16}O^-$, $^{12}C^{14}N^-$ and $^{13}C^{14}N^-$ in the first run (for C isotope and N/C mapping), and $^{16}O^-$, $^{12}C^{14}N^-$, $^{13}C^{14}N^-$, $^{52}Cr^{16}O^-$ and $^{56}Fe^{16}O^-$ in the second run (to determine associations of organic matter and heavy metals). Image processing and data analysis were carried out using the freeware package OpenMIMS (multi-isotope imaging mass spectrometry, freely available at http://nrims.harvard.edu). In total, more than eight NanoSIMS images were acquired from the labelled samples. More detailed information on $^{13}C$ isotopic maps and NanoSIMS image processing are provided in Supporting Information (SI)-A.

## 2.4.Fe plaque dissolution experiment

The function of root exudates in the dissolution of iron (hydr)oxides and release of their associated Cr into the medium was investigated in a time-lapse experiment. To this end, another set of plaque-bearing rice seedlings was exposed to Cr treatment (Fe80 × Cr(III)) and allowed to grow in the same nutrient solution for another 16 days. The sampling schedule was established for days 1, 3, 7, 10 and 16. Root samples at each sampling stage were subjected to DCB extraction for ICP readings of Fe, Cr and calcium (Ca).

### 2.5.Data analysis and statistics

All Cr-based computations were based on previously described equations (Liu et al., 2004; Zandi et al., 2020). The R statistical package (ver. 2.12.1) was used for all statistical analyses, and statistical differences between treatment means were assessed using the least significant difference (LSD) test at the 0.05 probability level (Data presented here are means ± SD, n=3).

## 3. Results

### 3.1.Fe and Cr concentrations in different root regions

Regardless of the examined root regions, the quantities of Fe and Cr adsorbed on IP (DCB extracts) in the roots treated with Cr were significantly higher than in the non-treated roots ($p < 0.05$) (Fig.1a,b). The observed discrepancies between Cr concentrations in DCB solutions extracted from different root sections were statistically significant ($p < 0.05$; DCB-Cr in mature root > root tip). Similarly, Cr concentrations in root tissues were in the following order: Root-Cr mature > Root-Cr tip ($p < 0.05$) (Fig.1b). Seedlings treated with Cr (+Cr seedlings) had higher Fe and Cr contents in their root tissues compared to non-treated counterparts, with markedly increased Fe accumulation in both the tip (2.25-fold) and mature root (1.72-fold) sections. It was also found that the overall Fe sequestration in IP (DCB-Fe) on the mature root surface was significantly higher compared to the tip region both under stress (Fe80-Cr(III)) and stress-free (Fe80-CK) conditions. Fe content in the root tip was significantly higher than in the mature root under Cr stress conditions (Fig.1a).

### 3.2. Fe and Cr concentrations/proportions in different rice parts

The respective concentrations of Cr and Fe in shoots, plaque-free roots, and DCB extracts differed in their distribution pattern. While the concentration (or relative proportion) of Cr in roots (53%) was significantly higher than that accumulated in IP (~37%) and shoots (~10%), the relative concentration of Fe in individual rice components was in the following order: DCB-extractable Fe > Root-Fe > Shoot-Fe (Table 1). Fe mainly accumulated in IP on the root surface under both stress (~89%) and stress-free (~91%) conditions. Irrespective of Cr levels applied, Fe concentration in

shoots did not show any significant differences, whereas Fe concentration in IP and roots of Cr-treated seedlings (Fe80-Cr(III)) was significantly (~1.52 to 1.98 times, respectively; $p$ <0.05) higher compared to non-Cr treated seedlings (Fe80-CK) (Table 1; Fig. S5a). Only 1.5% of the total Cr contents in roots translocated to shoots, with an 8.8% root-to-shoot Fe translocation efficiency observed in rice exposed to Cr treatment (Table 1).

### 3.3. Elemental distribution in rice root

#### *3.3.1.Two-dimensional surface view of the root tip and mature root sections*

The results of *in vivo* scanning of Fe and Cr deposits on the epidermal surface of the root tip (Fig. 2$a_{1-2}$) and mature root (Fig. 2$a_{4-5}$) sections were partially consistent with ICP-OES analyses concerning elemental distribution (Fig.1). The distribution patterns of Fe, Cr, and Ca fluorescence signals in the root tips after Fe80-Cr(III) treatment were relatively weak (low-intensity spots), with their hotspots scattered and located in slightly distant positions (Fig. 2$a_{4-6}$). Such distribution of elemental intensities was considerably different from that observed in the mature section of the root, where the intensity of elemental distribution mostly ranged from moderate (green), upper-moderate (yellow) to high (red) levels.

According to the results of correlation analysis, the element Cr showed a slightly low ($R^2$= 0.57) to rather high ($R^2$= 0.77) associations with high Fe intensities (~45-80 kilo-counts $s^{-1}$) and a range of low to moderate associations with Ca (~0.2-2.3 kilo-counts $s^{-1}$) intensities, respectively, in IP deposited in the tip zone of rice roots (Fig. 2$b_{4-5}$). Ca distribution pattern appeared to be similar to that of Fe in the mature root zone, signifying a strong linear association between Fe (~ 5-55 kilo-counts $s^{-1}$) and Ca (~ 0.15-25 kilo-counts $s^{-1}$) concentration intensities ($R^2$= 0.90; Fig. 2$b_3$). Similarly, Cr concentration was the highest in the mature root zone (Fig. 2$a_1$), and greatly co-localised with Ca ($R^2$= 0.91) and Fe ($R^2$= 0.90) intensities observed in the same root zone (Fig. 2$b_{1-2}$). The majority of Cr deposits in the mature zone of rice root was strongly correlated with a wide range of moderate (>50 kilo-counts $s^{-1}$) to high Fe intensities (<550 kilo-counts $s^{-1}$). Therefore, Cr was suggested to have a strong association with Fe concentration intensities in the mature zone of rice roots, and this mostly occurred in the Cr intensity range of ~10-38 kilo-counts $s^{-1}$ (Fig. 2$b_1$).

For Cr signals emitted from the upper surface of the root tip and mature root sections, several hotspots of moderate to high intensity were found, which were thought to be related to significant fractions of Cr sequestered in IP. As outlined above, the concentrations of Cr, Fe and Ca tended to be more intense in the mature root zone than in root tips. The majority of low to high Cr counts (~1.3 to 32.5 kilo-counts $s^{-1}$) correlated mostly with a low to moderate (~0.2-2.6 kilo-counts $s^{-1}$) counts of Ca intensities in the tip zone of rice roots after Cr treatment (Fig. 2$b_5$). Ca was mainly distributed on the epidermal surface of the mature root zone and this signal was reproduced by the element Fe. The lower correlation of Cr with Fe (Fig. 2$b_4$) to Ca (Fig. 2$b_5$) could also be attributed to the co-distribution of these two elements at hotspots, with no apparent correlation (or overlap) in their moderate-intensity spots. The result indicated that the correlation between the intensities of Fe and Ca fluorescence counts in root tips ($R^2$= 0.37) was considerably lower than that in mature roots ($R^2$= 0.90) under Fe80-Cr(III) treatment (Fig. 2$b_{3-6}$). The low correlation between Fe and Ca counts in root tips could be explained by a partial overlap of Fe hotspots in root tips in regions where Ca fluorescence intensity was high.

*3.3.2.Two-dimensional cross-section views of the root tip and mature root tissues*

Cr was mainly localised in the epidermal and exodermal layers of both rice root sections. A higher concentration of Cr was observed in the internal portion of sclerenchyma cells in the root tips in comparison to the mature root section (Fig. 3$a_{1-2}$). In other words, Cr was enriched (with more noticeable Cr spots) in the outer epidermis of mature roots. As shown in Fig. 3$b_1$, high-intensity Fe spots could be observed on the most distal sides of epidermal and exodermal cells, while moderate-intensity Fe spots were dispersed in sclerenchyma cells. In contrast, the inner portions of the exodermal layer in the tip section showed a higher Fe content than the epidermis (Fig. 3$b_2$). Moreover, Fe distribution was visible in root tip vessels, which likely corresponded to the vascular tissues of the root, implying that Fe could penetrate the root tip surface into the stele and move upward. However, there was no clear signal of Fe presence in the inner tissues of the mature root zone. Higher Fe concentrations were recorded on the epidermal surface of the mature root zone, as opposed to the root

tip zone after Fe80-Cr(III) treatment. This result was consistent with our root surface μ-XRF analysis, where an Fe-enrichment zone was observed on the dorsal surface of the mature root zone.

The co-occurrence of Fe and Cr in the epidermal and sclerenchyma cells was found in both root regions (Fig. 3$a_{1-2}$, $b_{1-2}$). The correlation of Fe and Cr deposition was more pronounced in the mature zone than the root tip zone, where, unlike the moderate amounts of Fe present in the root stele, no Cr was located in this region (Fig. S3). It can be suggested based on the overlapping Fe and Cr signals that there was a close correlation between Cr and Fe deposits in the epidermal and exodermal cell layers in both sections of rice roots.

Fig. 3$c_{1-2}$ illustrates the effect of Cr on S distribution in the root tip and mature root cross-sections. It is shown in Fig. 3$c_1$ that S was mainly dispersed in the outer cell layers (along the epidermis and exodermis), in the ground tissues (across the cortex and endodermis) and the stele (pericycle and vascular bundles) of the rice root. With the exception of the middle and central tissues, moderate-intensity S spots in the epidermis and exodermis layers correlated well with Fe hotspots (Fig. 3$b_{1-2}$; not marked), followed by Cr moderate-intensity spots. In comparison to Fig. 3$c_1$, a significant decrease in S accumulation was found across the epidermis and exodermis tissues of rice root tips (Fig. 3$c_2$). However, S distribution in the endodermis, pericycle, and stele of root tips was more extensive than in the mature root zone. This suggested that a considerable proportion of S could penetrate the stele in both sections of rice roots. Fig. 3$a_2$,$b_2$,$c_2$ demonstrated that S distribution did not follow the pattern observed for Fe and Cr in the outer cell layers of the root tip cross-section.

Potassium (K) and Ca primarily accumulated in the internal cell layers of both root sections, including endodermis, pericycle and vascular cylinder, as determined by high K and Ca fluorescence intensities (Fig. 3$e_{1-2}$,$f_{1-2}$). This observation suggested successful penetration of both elements into the root xylem and their subsequent possible translocation to the shoot. Images $e_1$,$f_1$ and $e_2$,$f_2$ in Fig. 3 clearly demonstrated that the cortex tissue in the mature root of Cr-exposed rice contained a limited degree of an irregular radial dispersion/gradient of K and Ca relative to the root tip zone. This result suggested that K and Ca tended to accumulate in vascular tissues. The distribution pattern of K was analogous to that of Ca in rice roots from both regions. Regardless of the Mn-free region in the cortex and Mn-enriched region in the stele, Mn concentration in the outer cell layers approximately

resembled Cr concentration in the rice root maturation region (Fig. 3$a_1$,$d_1$). Mn distribution in the rice root tip region was not only limited to the outer cell layers and stele, but also included parts of cortical tissues (Fig. 3$d_2$).

### 3.4. Cr K-edge μ-XANES analysis

One main peak and two shoulders, resolved at ~5999.0 eV (peak- 1), ~6005.0 eV (shoulder- 2) and ~6015.0 eV (shoulder- 3), respectively, were recorded in the Cr K-edge XANES spectra associated with spots of interest (SOIs) in the mature and tip region of the root (Fig. 4a). These features were more similar to Cr(III)-Fh and Cr(III)-FA standards rather than the Cr(III) acetate standards with a broader peak 1. The first derivative spectrum of Cr(III) acetate showed an apparently lower energy position of peak b compared to other standards and samples (Fig. 4b). In addition, peak b for all hotspot first derivative spectra displayed a similar shape to Cr(III)-Fh. However, peak c, which appeared in the first derivative spectra of Cr(III)-FA and all hotspots, was absent in Cr(III)-Fh. Therefore, Cr could co-exist and/or form complexes with fulvic acid-like (~FA) substances as an organic metabolite with more diverse functional groups (Qin et al., 2016; Wang et al., 2019; Zhang et al., 2020) and/or ferrihydrite as a typical amorphous form of iron (hydr)oxide in the outer cell layers of rice roots (Tripathi et al., 2014; Zandi et al., 2020).

LCF analysis based on spectral features (Fig. 4a) revealed that Cr(III) bound to FA-like anions accounted for 58-64% (spot 2-spot 1) and 13-17% (spot 2-spot 1) of total Cr in the tip and mature regions of rice roots, respectively (Fig. 4c). In other words, the epidermal layer (spot 1) of the mature root and the sub-epidermal layer (spot 1) in the root tip contained the highest proportion of Cr(III)-FA species compared to spot 2 in the corresponding layers. The outer cell layers of the root tip (spot 1 and spot 2) contained mainly Cr(III)-FA species, whereas Cr was mainly present as Fh-bound Cr(III) in the IP of the mature root outer cell layers (83-87% of total Cr). This result suggested that the immobilisation of Cr through complexation with ferrihydrite in IP on the outer cell layers of the mature root was more important than the immobilisation of Cr species by complexation with phyto-/organic metabolite compounds. More than 83% of total Cr was present as Cr(III)-Fh species in spot 1

and spot 2 of the mature root zone, which was considerably higher compared to spot 1 and spot 2 of the root tip zone.

### 3.5. Carbon isotope results

The mean $\delta^{13}C$ values showed a remarkable disparity between the plaque-free $^{13}C$-labelled (515.04‰) and non-labelled (-30.00‰) root samples (Table S2), indicating that the downward flux of photosynthetically processed $^{13}CO_2$ was significant (successful $^{13}C$ labelling) during the short period of our experiment. However, in terms of C concentrations in labelled/non-labelled roots, this discrepancy was not that robust since ~1.1% $^{13}C$ in the C pool of the non-labelled root samples was partially similar to ~1.7% $^{13}C$ in the C pool of the $^{13}C$-labelled roots. The results demonstrated that plants with IP on their roots tended to assimilate less $^{13}C$ out of $^{13}CO_2$ than plants devoid of plaque. We therefore found small differences between the $^{13}C$ abundance values in $^{13}C$-enriched root cells with or without IP induction. The severe reduction in C mass percentage (C%) in plaque-bearing roots compared to plaque-free roots was likely caused by the contribution of Fe (III) precipitates to the mass balance disturbance, regardless of whether roots were labelled or not.

The labelled shoot samples had a 3 times higher $^{13}C/^{12}C$ ratio (and $^{13}C$ abundance) compared to the non-labelled shoot samples. It should be noted that the existing differences in $\delta^{13}C$ and $^{13}C$ abundance between the labelled root and shoot samples did not significantly affect the mass percentage of C in the corresponding samples. In comparison with shoot tissues, root tissue (with or without IP) samples exposed to isotopically labelled $^{13}CO_2$ showed a lower proportion of $^{13}C$ isotope abundance, ranging from 49.9% to 51.9%. Another noteworthy aspect to consider was whether the presence of IP on the root surface altered C content in $^{13}C$-labelled roots. In this regards, our results demonstrated a substantial decrease (to about 49%) in C content of the plaque-bearing roots ($Fe^{13}C$-root) compared to plaque-free roots ($^{13}C$-root). It was assumed that the observed differences between the above samples could be associated with the release of metabolites into the culture medium, or even their lower production in the aerial parts, and thus decreased metabolic activity when IP was present.

### 3.6. Distribution mapping of metals and $^{13}C$ by NanoSIMS

NanoSIMS was used to map the relationship between metabolically active $^{13}C$-enriched root epidermal cells and metal complexes such as CrO and FeO (hereinafter referred to as iron (oxy) hydroxide mineral) in both the tip and mature root regions. Two selected areas of root tips (Fig. 5b) and mature roots (Fig. 5a) were analysed and colour composite images specifically showed the epidermal cell layer of the roots treated with ferrous-spiked solutions and Cr(III). Regions of interest in the two sections were defined based on whether iron (oxy) hydroxide minerals were present on (or within) the epidermal cell membrane. Comparison of the tip with the mature region allowed for accurate tracking of $^{13}C$-enriched metabolites in these two areas. The presence of $^{13}C$-enriched cells was more abundant in the epidermal cell layers of mature roots than in the root tips (Fig. 5).

Based on composite images showing relative locations of species, such as $^{52}Cr^{16}O$, $^{13}C^{14}N$ and $^{56}Fe^{16}O$, metabolically active epidermal cells in the mature root region were more enriched in $^{13}C$ metabolites compared to the root tip. The location of $^{13}C$-enriched metabolites was confined to the epidermal cell walls (area 1 in Fig. 5a,b) and apoplastic spaces (area 2 in Fig. S4$a_1$). It was also established that $^{13}C$-labelled metabolites in the above-specified spots co-localised with Fe and Cr. Moreover, $^{56}Fe^{16}O$ hotspots were always associated with a somewhat similar accumulation of $^{52}Cr^{16}O$. The $^{56}Fe^{16}O$ signal indicated that Fe was mainly located on the root epidermal surface, irrespective of the root zone. This phenomenon was more pronounced in the mature than in the immature (tip) region of the root, with the outer (excluding epidermis) and inner cell (ground tissues and stele) layers of the latter zone markedly associated with strong $^{56}Fe^{16}O$ signals (Fig. 3$b_2$).

The distribution of $^{56}Fe^{16}O$ in the two studied zones was heterogeneous with distinct regions of accumulation along the outer edge of the root epidermis (area 2 in Fig. 5a,b). The $^{16}O$ images in the two analysed zones clearly demonstrated that O signals were more evident in the mature root zone than in the root tips (Fig. S4). The general pattern of O distribution in $^{16}O$ images resembled the distribution observed in $^{56}Fe^{16}O$ and $^{52}Cr^{16}O$ images. Regardless of the root zone, the strongest $^{56}Fe^{16}O$ and $^{16}O$ signals originating from the outer epidermal cell wall layer were tightly linked with each other, implying that Fe was likely associated with oxide or oxy-hydroxide on the root surface. The presence of overlapping signals of $^{56}Fe^{16}O$ and $^{13}C^{14}N$ or $^{12}C^{14}N$ (organic carbons, OCs) in

specific locations on the root surface suggested the occurrence of organo-Fe oxyhydroxide co-precipitates (OFC) complexes in the examined root regions (SI-B).

### 3.7. Cr release during iron plaque dissolution

The mature root region appeared to have a lower Cr to Ca ratio compared to the root tips, regardless of the sampling time (Fig. 6). This discrepancy was attributed to the higher intensity of Ca distribution on the mature root surface (Fig. 2$a_{3\text{-}6}$). Fluctuations in the Fe/Ca ratios observed in the root tip were not statistically significant ($p > 0.05$), while a significant difference between the Fe/Ca ratios in the mature root zone (initial sharp decrease from day 1 to day 3) was recorded. The decrease in this region was followed by a slight insignificant increase (day 3-day 7) and then another decrease (day 7-day 10). This decline continued for the next 6 days (day 10-day 16). The trends in changes in the Cr/Ca ratios in each of the root sections were identical to those observed for the Fe/Ca ratios, suggesting that the release of immobilised Cr into the medium solution was consistent with IP dissolution.

## 4. Discussion

The results of the present work supported the hypothesis that plant exposure to Cr stress further stimulated $Fe^{2+}$ exclusion and oxidisation on the root surface (i.e., iron (hydr)oxide(s)/ IP formation) due to elevated root oxygen release or enzymatic oxidation (Table 1 ; Fig. S5a) (Briat et al., 2010). This effect was more confined to the mature zone of the rice root surface (Fig. 1a), presumably due to the more developed structure (Nishiuchi et al., 2012). Thus, this region could better limit Cr's bioavailability and mobility than immature root tips (Fig. 1b).

Iron (hydr)oxides serve not only as a physical barrier with a metal-sequestering ability (Amaral et al. (2017) but also as metal-chelating ligands (e.g., DMA: 2′-deoxymugenic acid), which can bind heavy metals (Banakar et al., 2017). This may explain why Fe accumulation in the tip zone was slightly higher than in the mature root zone under Cr stress (Fig. 1a).

Root Cr content was higher than in DCB extracts and shoots (Fig. 1b; Fig. S5b). This suggests that IP formation in conditions similar to flooded cultivation and its inhibitory effect on Cr uptake (Xiao et al., 2021) is not necessarily limited to the root epidermal surface (Fig. 2$a_{2-5}$). This condition most likely involves the apoplastic space in the outer layers of root cells (Fig. 3$b_{1-2}$) (Khan et al., 2016). It appears that Cr-induced increased aerenchyma-rhizosphere oxygen outflux, coinciding with higher Fe concentrations (Fig. 3$b_{1-2}$) (Becker et al., 2020), resulted in an increased amount of Cr precipitated on the outer cell layers compared to internal cell tissues in the tip and mature zone of rice roots (Fig. 3$a_{1-2}$). It's worth noting that increased Cr retention in outer cell layers of plaque-bearing roots compared to plaque-free roots was not associated with aerial uptake (Fig. S5b). This underlines the significance of IP in Cr immobilisation (Zandi et al., 2020, 2021).

The observed correlation between Cr and Ca concentration intensities in surface µ-XRF imaging of overlapping areas (Fig. 2$a_{1-3,}$ $a_{4-6,}$ $b_{2-5}$) indicated the importance of Ca as a critical factor in rigidifying cell walls and providing structural integrity to cellular membranes (Hepler, 2005; Pathak et al., 2021) in Cr cell wall sequestration by binding to it (Zeng et al., 2011). This effect was particularly restricted to the outer surface (i.e., epidermal layer) of the mature root zone, where similar Cr (Fig. 2$a_1$), Fe (Fig. 2$a_2$) and Ca (Fig. 2$a_3$) concentration intensities indicated the co-precipitation of Fe with Ca and Cr on epidermal root surfaces. It has been shown by sorption experiments that Ca (Gunnars et al., 2002; van Genuchten et al., 2014) and Cr (Yu et al., 2017) can react with surface hydroxyl groups and adsorb on iron oxides.

In the present study, Cr accumulation in the outer cell layers (except for the epidermis) was not associated with Cr deposition on cell walls (Fig. 3$a_{1-2}$), as indicated by the low correlation between Ca and Cr intensities ($R^2$= 0.01) in both root regions (Fig. S3). In contrast to our finding, in their research on arsenic (As) and Cr (VI), respectively, Xu et al. (2022) and Zeng et al. (2011) attributed the inhibitory role of cell walls to the entire root tissue. This difference might be related to the higher mobility of metal species used in their studies.

The formation of Fe and Mn plaque on rice roots is indeed a ROL (radial oxygen loss)-mediated exclusion strategy for limiting the absorption of potentially toxic elements (Yu et al., 2017; Li et al., 2019). Consistently with Crowder and Coltman (1993), Ye et al. (2001) and Zhang et al. (2015), the

concentration of Fe deposits in the outer cell layers of both root regions in this work was also more intense compared to Mn deposits (Fig. 3$b_{1-2}$,$d_{1-2}$). Therefore, it was not surprising that the co-occurrence of Fe and Cr deposits in hotspot and non-hotspot regions was more pronounced than that of Mn and Cr deposits in both regions of the root (Fig. 3; Fig. S3). It is generally accepted that the functional groups in IP have the potential to form a more active substrate for metal sequestration (Cao et al., 2018; Xu et al., 2018) than those in Mn plaque with its unique catalytic capacity and surface activity (Ye et al., 2001; Liu and Zhu, 2005). In addition to Fe and Mn plaques, sulphur (S) containing metabolites are also effective in Cr chelation and subcellular sequestration (Holland and Avery, 2011; Zandi et al., 2021), as was evident in simultaneous S and Cr depositions in the examined root regions (Fig.3$a_{1-2}$, $c_{1-2}$).

Exclusion and chelation mechanisms seem to co-occur in rice roots during Cr stress exposure, which may lead to decreased Cr entry into the inner layers of root cells and hence lowered Cr uptake, as seen in Fig. 3$a_{1-2}$ and Fig. S5b. This would confirm the hypothesis that root exudation of organic metabolites effectively reduces heavy metal uptake by rice at the root-rhizosphere interface (exclusion strategy) (Wang et al., 2019; Zhang et al., 2020).

The results of the XANES spectra of spots of interest (SOIs) in Cr µ-XRF mapping showed that phytometabolites involved in Cr chelation and detoxification were likely LMW fulvic acid-like (~FA) anions (Fig. 4c) (Wang et al., 2019; Zhang et al., 2020) which have not been reported for soil-free plant systems. These compounds are supposed to form stable chelate compounds with certain heavy metals (chelation strategy), such as Cd (Rashid et al., 2018) and Cr (Pradas del Real et al., 2014), enabling plants to withstand Cr-induced toxicity (Chen et al., 2017). Besides, reports indicated the high affinity of these metabolites for Fe(III) and other structurally similar trivalent metal cations, including Mn (III) (Tang et al., 2010; Saad et al., 2017).

The proportion of Cr(III)-FA complexes varied between individual SOIs (spot 1 and spot 2) in both root regions, proposing two different models (Fig. 4c). On the one hand, a higher percentage of phytometabolites or FA-like anions was bound to Cr(III) species adjacent to the root surface compared to the more internal tissues in the mature root (17% vs 13%), suggesting the existence of a resistance mechanism through exclusion (Osmolovskaya et al., 2018; Bali et al., 2020). On the other hand, a

reverse trend (58% and 64% for epidermal and subepidermal layers, respectively) was observed for organically bound Cr(III) in the root tip, suggesting the occurrence of a tolerance mechanism through inclusion and chelation. The proposed models were consistent with our IP dissolution results (Fig. 6). For instance, in the root tip zone with its unique trend of organo-Cr(III) species, neither IP dissolution nor Cr release was found to occur (Figs. 4c and 6; SI-C), reinforcing the possibility of Cr re-uptake from the root tip zone in the rhizosphere. Combining the proposed models with our ICP analysis (Fig. S5b), it can be inferred that the binding of FA-like anions to Cr(III) species did not lead to increased Cr mobility and accumulation in shoot tissues.

The limited IP build-up on the root surface (Fig. 2$a_5$) is assumed to have resulted in increased binding of FA-like anions relative to Fh species to Cr ions at the adsorbing sites in the root tip epidermis (58% vs 42%; T-Spot 2 in Fig. 4c). Consequently, the formed organo-Cr(III) species transferred to the immobilising sites in the outer cell layers of the root tip (Fig. 3$a_1$). This assumption was consistent with our carbon isotope results, where the absence (or scarcity) of root plaques increased the biosynthesis and transport of $^{13}$C-labelled organic metabolites (isotopic organic carbons-Ocs) to the root system (Table 2), thereby increasing the possibility of their binding to Cr. In a study by Tao et al. (2020), it was demonstrated that a small portion of assimilated $^{13}$C was incorporated in forming organic anion metabolites involved in Cd complexation.

The reduced abundance of isotopic OCs in rice roots with IP, compared to those stored in rice roots without IP, indicated that root plaques effectively prevented the assimilation and transfer of shoot-derived metabolites (Table 2) by Cr retention and stress alleviation. Studies on plaque-free roots revealed that heavy metal stress increased the content of organic acid anions in the roots and root exudates (Yang et al., 2000; Mariano Eduardo et al., 2005).

In contrast to being a more active site of organic anion metabolism and biosynthesis (Mariano Eduardo et al., 2005), only a small fraction of total Cr in individual SOIs in the outer cell layers of the mature root could be chelated (13-17%) or exuded by these metabolites compared to iron (hydr)oxides (Fig. 4c). There was an obvious dominance of the Cr(III)-Fh complexes relative to Cr(III)-FA complexes in individual SOIs in the mature root zone, indicating the substantial role played by Fh composition of iron (hydr)oxides in conferring higher tolerance to Cr toxicity through

chelation and immobilisation (Yu et al., 2017; Zandi et al., 2020) in this region. The reduced proportion of Cr(III)-Fh complexes in the epidermal layer of the mature root, relative to the subepidermal layer of the mature root (83% vs 87%; Fig. 4c), could be explained by a higher IP dissolution and its associated Cr under the influence of the supposed metabolites in this region (Fig. 6) (Sebastian and Prasad, 2016; Saad et al., 2017).

Root surface NanoSIMS imaging demonstrated how Fe oxyhydroxide (FeO) and Cr-induced isotopic/non-isotopic OCs were closely adherent to the epidermal surface and to each other (Fig. 5). This proximity in turn indicated adsorption of organic anion metabolites or occlusion in the interstices between amorphous Fh aggregates (Zeng et al., 2008). This co-occurrence not only inhibits the growth of Fh, but also tends to form smaller amorphous aggregates, and is therefore believed to affect aggregation behaviour, surface properties and solubility/accessibility of Fh (Eusterhues et al., 2014), contributing to Fh removal and its associated Cr from the root epidermal layer (Fig. 6). Previous dissolution studies showed that organic anion metabolites adsorbed on or co-precipitated with iron (hydr)oxides were likely to weaken Cr(III)-Fe(III)-(oxy)hydroxide compositional bonds under anaerobic conditions. This phenomenon enhanced the solubility and dissolution kinetics of iron (hydr)oxides and associated dissolved Cr (Saad et al., 2017).

It is worth noting that the relationship between the secretion/exudation rate of organic anions and their root concentrations is attributed to heavy metal-activated organic anion transporter channels in the plasma membrane of root cells (Yang et al., 2012). The observed varied patterns of Cr-induced secretion of phytometabolites (Fig. 5) and IP dissolutions (Fig. 6) between the examined root regions (mature root > root tip) could be due to the fact that root exudates, regardless of their role in heavy metal chelation (Montiel-Rozas et al., 2016), are secreted to promote solubility and absorption of poorly available nutrients in the rhizosphere (Jones et al., 2004; Gojon, 2013). Indeed, the mature zone of the root system is responsible for the majority of nutrient uptake in crop plants (Jones et al., 2004; Wirth et al., 2007; Gojon, 2013), which in turn explains the absolute predominance of root exudates and dissolution rate of iron (hydr)oxides in this region compared to the root tip region (Figs. 5 and 6). In other words, the increased secretion of organic anions from the mature region compared to the immature (tip) region of the root, in addition to destabilising iron (hydr)oxides (Yang et al.,

2012, 2013) and possible release of their co-precipitated Cr ions (Fig. 6), can also be considered an essential mechanism reducing the physical resistance of root plaques to nutrient absorption.

Considering the absence of IP dissolution and release of its Cr co-precipitates (Fig. 6) and limited secretion of organic anions (Fig. 5) in the root tip region, the relatively higher proportion of organo-Cr(III) species in more internal than external tissues (64% vs 58%) of the outer cell layers in this region (Fig. 4c), likely reflected the importance of organic anions (i.e., FA-like anions) in capturing and transferring the absorbed Cr in the form of organo-Cr(III) species to the root tip sub-epidermis. The proposed model can also be construed as a possible direct or indirect re-uptake of Cr from the solution medium after release from the mature region of rice roots (as outlined earlier) and its subsequent immobilisation by a combination of Fh and FA-like chelators. The strong presence of organo-Cr(III) (58-64%) complexes in relation to Cr(III)-Fh (36-42%) complexes in the root tip outer cell layers (Fig. 4c) was an indirect reference to the reinforcing role of FA-like anions in Cr chelation and immobilisation when the Fh chelator pool was insufficient. As indicated earlier, the accumulation of $^{13}$C-labelled organic metabolites was more intense in plaque-free roots ($^{13}$C-root) than in plaque-bearing roots (Fe$^{13}$C-root) under Cr stress, regardless of the root section (Table 2). This indirectly underscored the role played by these anions as complementary factors for Cr immobilisation.

## 5. Concluding remarks

The present study concludes that root plaques have a central role in Cr chelation and immobilisation, especially in the mature root region. The uptake inhibiting function of IP was not only confined to root epidermal surfaces but also stretched across the entire root outer cell layers. It strongly suggested that an integration of both Cr resistance (exclusion) and tolerance (chelation) strategies was directly involved in the mature region of the root, where iron (hydr)oxide precipitates alone accounted for over 83% of total Cr (Cr(III)-Fh) species at Cr hotspots in the epidermal and sub-epidermal layers of root cells. An uneven partnership in root Cr retention and inactivation was actively present in root tissues; as such, none or limited IP coated roots contained an increased amount of isotopic OCs or a higher percentage of Cr(III)-FA species (58-64% for root tips), respectively. The

proposed model concerning the outflow (Pos. mature root) or inflow (Neg. root tips) of metabolites carrying Cr (organo-Cr (III)) in outer cell layers of both root regions was well consistent (positive-Pos./ negative- Neg. effect) with signal intensities of $^{13}C$-labelled spots as active nano-scaled spots of root exudates and iron (hydr)oxide dissolution.

## Data availability

In addition to the SI, all other reasonable requests for data and research materials are available via contacting the corresponding author.

## Funding

The work was funded by the Top-Notch Young Talents Program of China, the National Natural Science Foundation of China (U1632134), the Agricultural Science and Technology Innovation Program of the Chinese Academy of Agricultural Science (2021-2025) and the National Center for Scientific Research (CNRS) in France (CNRS funded the NanoSIMS analyses). The National NanoSIMS facility at the Muséum National d'Histoire Naturelle was established by funds from CNRS, Région Ile de France, Ministère délégué à l'Enseignement Supérieur et à la Recherche, and the Muséum National d'Histoire Naturelle. Synchrotron-based microprobe analysis was conducted at the Canadian Light Source, a national research facility of the University of Saskatchewan, which is supported by the Canada Foundation for Innovation, the Natural Sciences and Engineering Research Council of Canada, the National Research Council of Canada, the Canadian Institutes of Health Research, the Province of Saskatchewan, and the University of Saskatchewan.

## CRediT authorship contribution statement

#XX and PZ equally contributed to this work.

**JY**: designed the experiments. **XX** and **PZ**: performed the lab experiments with the kind guidance of JY. **JY**, **XX** and **PZ**: performed the XRF, XANES and SEM measurements and data analysis. **JY**, **JL**, **RL** and **CR**: conducted the NanoSIMS experiments. **JY**, **JL** and **XX**: performed the

NanoSIMS data analysis. **PZ**, XX, **JY** and **JL**: analysed the data and drafted the manuscript. **JY**, **PZ**, **BE**, **ES** and **BBK**: participated in the interpretation of results. **JY**, **CR**, **RL**, **PZ**, **BE**, **ES** and BBK: improved the grammar and corrected spelling mistakes. **PZ**, **JY**, XX, **BE**, **BBK** and **ES**: edited and thoroughly revised the manuscripts. All authors read, corrected and approved the final submitted version of the manuscript.

## Declaration of Competing Interest

The authors declare that they have no known competing financial interests or personal relationships that could have appeared to influence the work reported in this paper.

## References


Agnello, A., Huguenot, D., Van Hullebusch, E., Esposito, G., 2014. Enhanced phytoremediation: a review of low molecular weight organic acids and surfactants used as amendments. Crit. Rev. Environ. Sci. Technol. 44, 2531e2576. https://dx.doi.org/10.1080/10643389.2013.829764.

Ali, W., Zhang, H., Mao, K., Shafeeque, M., Aslam, M.W., Yang, X., Zhong, L., Feng, X., Podgorski, J., 2022. Chromium contamination in paddy soil-rice systems and associated human health risks in Pakistan. Sci. Total Environ. 826,153910. https://doi.org/10.1016/j.scitotenv.2022.153910.

Amaral, D.C., Lopes, G., Guilherme, L.R.G., Seyfferth, A.L., 2017. A new approach to sampling intact Fe plaque reveals Si-induced changes in Fe mineral composition and shoot as in rice. Environ. Sci. Technol. 51, 38–45. https://doi.org/10.1021/acs.est.6b03558

Assimakopoulou, A., Kotsiras, A., Nifakos, K., 2013. Incidence of lettuce tipburn as related to hydroponic system and cultivar. J. Plant Nutr. 36(9), 1383–1400. https://doi.org/10.1080/01904167.2013.793709

Bali, A.S., Sidhu, G.P.S., Kumar, V., 2020. Root exudates ameliorate cadmium tolerance in plants: A review. Environ. Chem. Lett. 18, 1243–1275. https://doi.org/10.1007/s10311-020-01012-x

Banakar, R., Fernandez, A.A., Díaz-Benito, P., Abadia, J., Capell, T., Christou, P., 2017. Phytosiderophores determine thresholds for iron and zinc accumulation in biofortified rice

659 endosperm while inhibiting the accumulation of cadmium. J. Exp. Bot. 68(17), 4983–
660 4995. https://doi.org/10.1093/jxb/erx304
661 Becker, M., Ngo, N.S., Schenk, M.K.A., 2020. Silicon reduces the iron uptake in rice and induces
662 iron homeostasis related genes. Sci. Rep. 10, 5079. https://doi.org/10.1038/s41598-020-61718-4
663 Briat, J.F., Ravet, K., Arnaud, N., Duc, C., Boucherez, J., Touraine, B., Cellier, F., Gaymard, F., 2010.
664 New insights into ferritin synthesis and function highlight a link between iron homeostasis and
665 oxidative stress in plants. Ann. Bot. 105, 811–822. https://doi.org/10.1093/aob/mcp128
666 Cao, Z.Z., Qin, M.L., Lin, X.Y., Zhu, Z.W., Chen, M.X., 2018. Sulfur supply reduces cadmium
667 uptake and translocation in rice grains (*Oryza sativa* L.) by enhancing iron plaque formation,
668 cadmium chelation vacuolar sequestration. Environ. Pollut. 238, 76–84.
669 https://doi.org/10.1016/j.envpol.2018.02.083
670 Chen, K., Li, B., He, G., 2000. High-yielding cultivation techniques for a new high-quality rice
671 variety Xiangzaoxian No. 31. Crop Res. 4, 43. https://doi.org/10.16848/j.cnki.issn.1001-
672 5280.2000.04.017. [in Chinese]
673 Chen, Y.T., Wang, Y., Yeh, K.C., 2017. Role of root exudates in metal acquisition and tolerance.
674 Curr. Opin. Plant Biol. 39, 66–72. https://doi.org/10.1016/j.pbi.2017.06.004
675 Cheng, H., Wang, M., Wong, M.H., Ye, Z., 2014. Do radial oxygen loss and iron plaque formation
676 on roots alter Cd and Pb uptake and distribution in rice plant tissues? Plant Soil 375, 137–148.
677 https://doi.org/10.1007/s11104-013-1945-0
678 Coudert, Y., Périn, C., Courtois, B., Khong, N.G., Gantet, P., 2010. Genetic control of root
679 development in rice, the model cereal. Trend Plant Sci. 15(4), 219–226. https://doi.org/
680 10.1016/j.tplants.2010.01.008.
681 Crowder, A.A., Coltman, D.W., 1993. Formation of manganese oxide plaque on rice roots in solution
682 culture under varying pH and manganese ($Mn^{2+}$) concentration conditions. J. Plant Nutr. 16 (4),
683 589–599. https://doi.org/10.1080/01904169309364559
684 Deng, D., Wu, S.C., Wu, F.Y., Deng, H., Wong, M.H., 2010. Effects of root anatomy and Fe plaque
685 on arsenic uptake by rice seedlings grown in solution culture. Environ. Pollut. 158, 2589–2595.
686 https://doi.org/10.1016/j.envpol.2010.05.015.

687 Eusterhues, K., Hädrich, A., Neidhardt, J., Küsel, K., Keller, T.F., Jandt, K.D., Totsche, K.U., 2014.
688 Reduction of ferrihydrite with adsorbed and coprecipitated organic matter: microbial reduction
689 by Geobacter bremensisvs. Abiotic reduction by Na-dithionite. Biogeosciences 11, 4953–4966.
690 https://doi.org/10.5194/bg-11-4953-2014
691 Frommer, J., Voegelin, A., Dittmar, J., Marcus, M.A., Kretzschmar, R., 2011. Biogeochemical
692 processes and arsenic enrichment around rice roots in paddy soil: results from micro-focused X-
693 ray spectroscopy. Eur. J. Soil Sci. 62, 305–317. https://doi.org/10.1111/j.1365-
694 2389.2010.01328.x
695 Fukao, T., Barrera-Figueroa, B.E., Juntawong, P., Peña-Castro, J.M., 2019. Submergence and
696 waterlogging stress in plants: a review highlighting research opportunities and understudied
697 aspects. Front. Plant Sci. 10, 340. https://doi.org/10.3389/fpls.2019.00340
698 Ge, T., Yuan, H., Zhu, H., Wu, X., Nie, S., Liu, C., Tong, C., Wu, J., Brookes, P., 2012. Biological
699 carbon assimilation and dynamics in a flooded rice–soil system. Soil Biol. Biochem. 48, 39–46.
700 https://doi.org/10.1016/j.soilbio.2012.01.009
701 Geng, Z., Wang, P., Fu, Y.,Liu, W., Cui, Y., 2020. Bioaccessibility of chromium in rice and Its
702 human health risk assessment, Asian J. Ecotoxicol. (6), 205–211.
703 https://doi.org/10.7524/AJE.1673-5897.20190610002
704 Gojon, A., 2013. Inorganic Nitrogen acquisition and signalling. In: Eshel, A., Beeckman, T. (Eds.),
705 Plant Roots. CRC Press, Boca Rotan, pp. 1–14.
706 Gu, D., Zhen, F., Hannaway, D.B., Zhu, Y., Liu, L., Cao, W., Tang, L., 2017. Quantitative
707 classification of rice (*Oryza sativa* l.) root length and diameter using image analysis. PLoS One
708 12(1), e0169968. https://doi.org/10.1371/journal.pone.0169968.
709 Gunnars, A., Blomqvist, S., Johansson, P., Andersson, C., 2002. Formation of Fe (III) oxyhydroxide
710 colloids in fresh water and brackish seawater, with incorporation of phosphate and calcium.
711 Geochim. Cosmochim. Acta 66, 745–758. https://doi.org/10.1016/S0016-7037(01)00818-3
712 Hayat, S., Khalique, G., Irfan, M., Wani, A.S., Tripathi, B.N., Ahmad, A., 2012. Physiological
713 changes induced by chromium stress in plants: an overview. Protoplasma 249, 599–611.
714 https://doi.org/10.1007/s00709-011-0331-0

715 Hepler, P.K., 2005. Calcium: A central regulator of plant growth and development. Plant Cell. 17(8),
716 2142–2155. https://doi.org/10.1105/tpc.105.032508
717 Holland, S.L., Avery, S.V., 2011. Chromate toxicity and the role of sulfur. Metallomics 3, 1119–1123.
718 https://doi.org/10.1039/c1mt00059d
719 Holzschuh, M.J., Carlos, F.S., Carmona, F.C., Bohnen, H., Anghinoni, I., 2014. Iron oxidation on the
720 surface of adventitious roots and its relation to aerenchyma formation in rice genotypes. Revista
721 Brasileira de Ciência do Solo 38 (1), 185–192. https://doi.org/10.1590/S0100-
722 06832014000100018
723 Hu, Y., Huang, Y.Z., Liu Y.X., 2014. Influence of iron plaque on chromium accumulation and
724 translocation in three rice (*Oryza sativa* L.) cultivars grown in solution culture. Chem. Ecol. 30
725 (1), 29–38. https://doi.org/10.1080/02757540.2013.829050
726 Jones, D.L., Hodge, A., Kuzyakov, Y., 2004. Plant and mycorrhizal regulation of
727 rhizodeposition. New Phytol. 163 (3), 459–480. https://doi.org/10.1111/j.1469-
728 8137.2004.01130.x
729 Kaiser, C., Kilburn, M.R., Clode, P.L., Fuchslueger, L., Koranda, M., Cliff, J.B., Solaiman, Z.M.,
730 Murphy, D.V., 2015. Exploring the transfer of recent plant photosynthates to soil microbes:
731 mycorrhizal pathway vs. direct root exudation. New Phytol. 205, 1537–1551.
732 https://doi.org/10.1111/nph.13138
733 Khan, F.H., Ambreen, K., Fatima, G. and Kumar, S., 2012. Assessment of health risks with reference
734 to oxidative stress and DNA damage in chromium exposed population. Sci. Total Environ. 430,
735 68–74. https://doi.org/10.1016/j.scitotenv.2012.04.063
736 Khan, N., Seshadri, B., Bolan, N., Saint, C.P., Kirkham, N.B., Chowdhury, S., Yamaguchi, N., Lee,
737 D.Y., Li, G., Kunhikrishnan, A., Qi, F., Karunanithi, R., Qiu, R., Zhu, Y.G., Syu, C.H., 2016.
738 Root iron plaque on wetland plants as a dynamic pool of nutrients and contaminants. Adv. Agron.
739 138, 1–96. https://doi.org/10.1016/bs.agron.2016.04.002
740 Li, J., Jia, Y., Dong, R., Huang, R., Liu, P., Li, X., Wang, Z., Liu, G., Chen. Z., 2019. Advances in the
741 mechanisms of plant tolerance to manganese toxicity. Int. J. Mol. Sci. 20(20), 5096.

https://doi.org/10.3390/ijms20205096

Li., Y., Zhao, J., Zjang, B., Liu, Y., Xu, X., Li, Y.F., Li, B., Gao, Y., Chai, Z., 2015. The influence of iron plaque on the absorption, translocation and transformation of mercury in rice (*Oryza sativa* L.) seedlings exposed to different mercury species. Plant Soil 398, 87–97. https://doi.org/10.1007/s11104-015-2627-x

Liu, W.J., Zhu, Y.G., 2005. Iron and Mn plaques on the surface of roots of wetland plants. Acta Ecol. Sin. 25 (2), 358–363. (In Chinese)

Liu, W.J., Zhu, Y.G., Smith, F.A., Smith, S.E., 2004. Do phosphorus nutrition and iron plaque alter arsenate (As) uptake by rice seedlings in hydroponic culture? New Phytol. 162, 481–488. https://doi.org/10.1111/j.1469-8137.2004.01035.x

Lombi, E., Susini, J., 2009. Synchrotron-based techniques for plant and soil science: opportunities, challenges and future perspectives. Plant Soil 320, 1–35. https://doi.org/10.1007/s11104-008-9876-x

Lu, L., Xie, R., Liu, T., Wang, H., Hou, D., Du, Y., He, Z., Yang, X., Sun, H., Tian, S., 2017. Spatial imaging and speciation of Cu in rice (*Oryza sativa* L.) roots using synchrotron-based X-ray microfluorescence and X-ray absorption spectroscopy. Chemosphere 175, 356–364. https://doi.org/10.1016/j.chemosphere.2017.02.082.

Luo, Q., Wang, S., Sun, L., Wang, H., 2017. Metabolic profiling of root exudates from two ecotypes of *Sedum alfredii* treated with Pb based on GC-MS. Sci. Rep. 7, 39878. https://doi.org/10.1038/srep39878

Mariano Eduardo, D., Jorge Renato, A., Keltjens Willem, G., Marcelo, M., 2005. Metabolism and root exudation of organic acid anions under aluminium stress. Braz. J. Plant Physiol. 17, 157–172. https://doi.org/10.1590/S1677-04202005000100013.

Montiel-Rozas, M.M., Madejón, E., Madejón, P., 2016. Effect of heavy metals and organic matter on root exudates of herbaceous species: An assessment in sand and soil conditions under different levels of contamination. Environ. Pollut. 216, 273–281. https://doi.org/10.1016/j.envpol.2016.05.080

Nickens, K.P., Patierno, S.R. and Ceryak, S., 2010. Chromium genotoxicity: a double-edged sword.

Chem. Biol. Interact., 188(2), 276–288. https://doi.org/10.1016/j.cbi.2010.04.018

Nishiuchi, S., Yamauchi, T., Takahashi, H., Kotula, L., Nakazono, M., 2012. Mechanisms for coping with submergence and waterlogging in rice. Rice 5, 2. https://doi.org/10.1186/1939-8433-5-2

Osmolovskaya, N., Dung, V.V., Kuchaeva, L., 2018. The role of organic acids in heavy metal tolerance in plants. Bio. Comm. 63 (1), 9–16. https://doi.org/10.21638/spbu03.2018.103

Pathak, R.K., Singh, D.B., Sharma, H., Pandey, D., Dwivedi, S., 2021. Calcium uptake and translocation in plants. In: Upadhyay, S.K. (Ed.), Calcium Transport Elements in Plants, 1st, ed. Academic Press, New York, pp. 373–386.

Peng, C., Duan, D., Xu, C., Chen, Y., Sun, L., Zhang, H., Yuan, X., Zheng, L., Yang, Y., Yang, J., Zhen, X., Chen, Y., Shi, J., 2015. Translocation and biotransformation of CuO nanoparticles in rice (*Oryza sativa* L.) plants. Environ. Pollut. 197, 99–107. https://doi.org/10.1016/j.envpol.2014.12.008.

Pradas del Real, A.E., García-Gonzalo, P., Lobo, M.C., Pérez-Sanz, A., 2014. Chromium speciation modifies root exudation in two genotypes of *Silene vulgaris*. Environ. Exp. Bot. 107, 1−6. https://doi.org/10.1016/j.envexpbot.2014.05.002

Qin, Y., Zhu, H., Zhang, M., Zhang, H., Xiang, C., Li, B., 2016. GC-MS analysis of membrane-graded fulvic acid and Its activity on promoting wheat seed germination. Molecules 21(10), 1363. https://doi.org/10.3390/molecules21101363

Rashid, I., Murtaza, G., Zahir, Z.A., Farooq, M., 2018. Effect of humic and fulvic acid transformation on cadmium availability to wheat cultivars in sewage sludge amended soil. Environ. Sci. Pollut. Res. 25, 16071–16079. https://doi.org/10.1007/s11356-018-1821-9.

Ravel, B., Newville, M., 2005. Athena, Artemis, Hephaestus: data analysis for X-ray absorption spectroscopy using IFEFFIT. J. Synchrotron Rad. 12, 537–541. https://doi.org/10.1107/S0909049505012719

Saad, E.M., Sun, J., Chen, S., Borkiewicz, O.J., Zhu, M., Duckworth, O.W., Tang, Y., 2017. Siderophore and organic acid promoted dissolution and transformation of Cr(III)-Fe (III)-(oxy) hydroxides. Environ. Sci. Technol. 51 (6), 3223–3232. https://doi.org/10.1021/acs.est.6b05408

Seal, A.N., Haig, T., Pratley, J.E., 2004. Evaluation of putative allelochemicals in rice root exudates for their role in the suppression of Arrowhead root growth. J. Chem. Ecol. 30, 1663–1678. https://doi.org/10.1023/B:JOEC.0000042075.96379.71

Sebastian, A., Prasad, M.N.V., 2016. Iron plaque decreases cadmium accumulation in *Oryza sativa* L. and serves as a source of iron. Plant Biol. 18 (6), 1008–1015. https://doi.org/10.1111/plb.12484.

Seyfferth, A.L., Webb, S.M., Andrews, J.C., Fendorf, S., 2010. Arsenic localization, speciation, and co-occurrence with iron on rice (*Oryza sativa* l.) roots having variable Fe coatings. Environ. Sci. Technol. 44, 8108–8113. https://doi.org/10.1021/es101139z

Somenahally, A.C., Hollister, E.B., Yan, W., Gentry, T.J., Loeppert, R.H., 2011. Water management impacts on arsenic speciation and iron-reducing bacteria in contrasting rice-rhizosphere compartments. Environ. Sci. Technol. 45, 8328–8335. https://doi.org/10.1021/es2012403

Tang, Y.Z., Michel, F.M., Zhang, L.H., Harrington, R., Parise, J.B., Reeder, R.J., 2010. Structural properties of the Cr(III)-Fe(III) (oxy)hydroxide compositional series: Insights for a Nanomaterial "solid solution". Chem. Mat. 22 (12), 3589–3598. https://doi.org/10.1021/cm1000472

Tao, Q., Zhao, J., Jinxing, L., Liu, Y., Luo, J., Yuan, S., Li, B., Li, Q., Xu, Q., Yu, X., Huang, H., Li, T., 2020. Unique root exudate tartaric acid enhanced cadmium mobilization and uptake in Cd-hyperaccumulator *Sedum alfredii*. 383, 121177. https://doi.org/10.1016/j.jhazmat.2019.121177

Tian, S., Lu, L., Yang, X., Webb, S.M., Du, Y., Brown, P.H., 2010. Spatial imaging and speciation of lead in the accumulator plant *Sedum alfredii* by microscopically focused synchrotron X-ray investigation. Environ. Sci. Technol. 44(15), 5920–5926. https://doi.org/10.1021/es903921t

Tripathi, R.D., Tripathi, P., Dwivedi, S., Kumar, A., Mishra, A., Chauhan, P.S., Norton, G.J., Nautiyal, C.S., 2014. Roles for root iron plaque in sequestration and uptake of heavy metals and metalloids in aquatic and wetland plants. Metallomics 6, 1789–1800. https://doi.org/10.1039/c4mt00111g

Uren, N.C., 2000. Types, amount, and possible functions of compounds released into the rhizosphere by soil-grown plants. In: Pinton, R., Varanini, Z., Nannipieri, P. (Eds.), The

Rhizosphere: Biochemistry and Organic Substances at the Soil–Plant Interface. Marcel Dekker, New York, pp. 19–40.

van Genuchten, C.M., Gadgil, A.J., Peña, J., 2014. Fe (III) nucleation in the presence of bivalent 12 cations and oxyanions leads to subnanoscale 7 Å polymers. Environ. Sci. Technol. 48, 11828–11836. https://doi.org/10.1021/es503281a

Wang, Y., Yang, J., Han, H., Hu, Y., Wang, J., Feng, Y., Yua, B., Xia, X., Darma, A., 2021. Differential transformation mechanisms of exotic Cr(VI) in agricultural soils with contrasting physio-chemical and biological properties. Chemosphere 729, 130546 https://doi.org/10.1016/j.chemosphere.2021.130546

Wang, Y., Yang, R., Zheng, J., Shen, Z., Xu, X., 2019. Exogenous foliar application of fulvic acid alleviate cadmium toxicity in lettuce (*Lactuca sativa* L.). Ecotoxicol. Environ Saf. 167,10–19. https://doi.org/10.1016/j.ecoenv.2018.08.064.

Williams, P.N., Santner, J., Larsen, M., Lehto, N.J., Oburger, E., Wenzel, W., Glud, R.N., Davison, W., Zhang, H., 2014. Localised flux maxima of arsenic, lead, and iron around root apices in flooded lowland rice. Environ. Sci. Technol. 48 (15), 8498–8506. https://doi.org/10.1021/es501127k

Wirth, J., Chopin, F., Santoni, V., Viennois, G., Tillard, P., Krapp, A., Lejay, L., Daniel-Vedele, F., Gojon, A., 2007. Regulation of root nitrate uptake at the NRT2.1 protein level in *Arabidopsis thaliana*. J. Biol. Chem. 282, 23541–23552. https://doi.org/10.1074/jbc.M700901200

Wu, C., Ye, Z., Li, H., Wu, S., Deng, D., Zhu, Y., Wong, M., 2012. Do radial oxygen loss and external aeration affect iron plaque formation and arsenic accumulation and speciation in rice? J. Exp. Bot. 63, 2961–2970. https://doi.org/10.1093/jxb/ers017.

Xiao, W., Ye, X., Zhu, Z., Zhang, Q., Zhao, S., Chen, D., Gao, N., Hu, J., 2021. Continuous flooding stimulates root iron plaque formation and reduces chromium accumulation in rice (*Oryza sativa* L.). Sci. Total Environ. 788,147786. https://doi.org/10.1016/j.scitotenv.2021.147786

Xiao, W., Zhang, Q., Zhao, S., Chen, D., Gao, N., Huang, M., Ye, X., 2023. Citric acid secretion from rice roots contributes to reduction and immobilization of Cr(VI) by

driving microbial sulfur and iron cycle in paddy soil. Sci. Total Environ.16,158832. https://doi.org/10.1016/j.scitotenv.2022.158832.

Xu, B., Wang, F., Zhang, Q., Lan, Q., Liu, C., Guo, X., Cai, Q., Chen, Y., Wang, G., Ding, J., 2018. Influence of iron plaque on the uptake and accumulation of chromium by rice (*Oryza sativa* L.) seedlings: Insights from hydroponic and soil cultivation. Ecotoxicol Environ. Saf. 162, 51–58. https://doi.org/10.1016/j.ecoenv.2018.06.063

Xu, B., Yu, S., 2013. Root iron plaque formation and characteristics under N2 flushing and its effects on translocation of Zn and Cd in paddy rice seedlings (*Oryza sativa*). Ann. Bot., 111(6):1189–1195. doi:10.1093/aob/mct072

Xu, M., Gao, P., Wu, J., Ma, J., Zhang, X., Yang, G., Long, L., Chen, C., Song, C., Xiao, Y., 2022. Biochar promotes arsenic sequestration on iron plaques and cell walls in rice roots. Chemosphere 288, 132422. https://doi.org/10.1016/j.chemosphere.2021.132422

Yamaji, N., Ma, J.F., 2007. Spatial distribution and temporal variation of the rice silicon transporter Lsi1. Plant Physiol. 143, 1306–1313. https://doi.org/10.1104/pp.106.093005

Yang, J., Xia, X., Liu, J., Wang, J., Hu, Y., 2020. Molecular mechanisms of chromium (III) immobilization by organo–ferrihydrite co-precipitates: The significant roles of ferrihydrite and carboxyl. Environ. Sci. Technol. 54 (8), 4820–4828. https://doi.org/10.1021/acs.est.9b06510

Yang, J., Zhu, S., Zheng, C., Sun, L., Liu, J., Shi, J., 2015. Impact of S fertilizers on pore-water Cu dynamics and transformation in a contaminated paddy soil with various flooding periods. J. Hazard. Mater. 286, 432–439. https://doi.org/10.1016/j.jhazmat.2015.01.035

Yang, L.T., Jiang, H.X., Qi, Y.P., Chen, L.S., 2012. Differential expression of genes involved in alternative glycolytic pathways, phosphorus scavenging and recycling in response to aluminium and phosphorus interactions in citrus roots. Mol. Biol. Rep. 39 (5), 6353–6366. https://doi.org/10.1007/s11033-012-1457-7.

Yang, L.T., Qi, Y.P., Jiang, H.X., Chen, L.S., 2013. Roles of organic acid anion secretion in aluminium tolerance of higher plants. Biomed. Res. Int. 2013, 173682. https://doi.org/10.1155/2013/173682

Yang, S., Zhao, J., Chang, S.X., Collins, C., Xu, J., Liu, X., 2019a. Status assessment and probabilistic health risk modeling of metals accumulation in agriculture soils across China: A synthesis. Environ. Int. 128, 165–174. https://doi.org/10.1016/j.envint.2019.04.044

Yang, Y., Yang, Z., Yu, S., Chen, H., 2019b. Organic acids exuded from roots increase the available potassium content in the rhizosphere soil: a rhizobag experiment in *Nicotiana tabacum*. *Hort. Sci. 54*, 23–27. https://doi.org/10.21273/HORTSCI13569-18

Yang, Y.Y., Jung, J.Y., Song, W.Y., Suh, H.S., Lee, Y., 2000. Identification of rice varieties with high tolerance or sensitivity to lead and characterization of the mechanism of tolerance. Plant Physiol. 124, 1019–1026. https://doi.org/10.1104/pp.124.3.1019

Ye, Z.H., Cheung, K.C., Wong, M.H., 2001. Copper uptake in *Typha latifolia* as affected by iron and manganese plaque on the root surface. Can. J. Bot. 79, 314–320. https://doi.org/10.1139/b01-012

Yu, X.Z., Lu, M.R., Zhang, X.H., 2017. The role of iron plaque in transport and distribution of chromium by rice seedlings. Cereal Res. Commun. 45 (4), 598–609. https://doi.org/10.1556/0806.45.2017.040

Yu, Y., 2018. History of Chinese Rice Varieties (Hunan Conventional Rice Rolls), first ed. China Agriculture Press, China.

Yuan, H., Zhu, Z., Liu, S., Ge, T., Jing, H., Li, B., Liu, Q., Lynn, T.M., Wu, J., Kuzyakov, Y., 2016. Microbial utilization of rice root exudates: 13C labeling and PLFA composition. Biol. Fertil. Soils 52, 615–627. https://doi.org/10.1007/s00374-016-1101-0

Zandi, P., Yang, J., Darma, A., Bloem, E., Xia, X., Wang, Y., Li, Q., Schnug, E., 2022. Iron plaque formation, characteristics, and its role as a barrier and/or facilitator to heavy metal uptake in hydrophyte rice (*Oryza sativa* L.). Environ. Geochem. Health. https://doi.org/10.1007/s10653-022-01246-4.

Zandi, P., Yang, J., Xia, X., Barabasz-Krasny, B., Możdżeń, K., PuŁa, J., Elke, B., Wang, Y., Hussain, S., Hashemi, S.M., Różanowski, B., Qian, L., 2021. Sulphur nutrition and iron plaque formation on roots of rice seedlings and their consequences for immobilisation and uptake of chromium in solution culture. Plant Soil 462, 365–388. https://doi.org/10.1007/s11104-021-04870-8

Zandi, P., Yang, J.J., Xin, X., Yu, T., Li, Q., Możdżeń, K., Barabasz-Krasny, B., Yaosheng, W., 2020. Do sulfur addition and rhizoplane iron plaque affect chromium uptake by rice (*Oryza sativa* L.) seedlings in culture solution? J. Hazard. Mater. 2020, 121803. https://doi.org/10.1016/j.jhazmat.2019.121803

Zeng, F., Chen, S., Miao, Y., Wu, F., Zhang, G., 2008. Changes of organic acid exudation and rhizosphere pH in rice plants under chromium stress. Environ. Pollut. 155 (2), 284–289. https://doi.org/10.1016/j.envpol.2007.11.019

Zeng, F., Zhou, W., Qiu, B., Ali, S.,Wu, F., Zhang, G., 2011. Subcellular distribution and chemical forms of chromium in rice plants suffering from different levels of chromium toxicity. J. Plant Nutr. Soil Sci. 174, 249–256. https://doi.org/10.1002/jpln.200900309

Zhang, Q., Liu, J., Lu, H., Zhao, S., Wang, W., Du, J., Yan, C., 2015. Effects of silicon on growth, root anatomy, radial oxygen loss (ROL) and Fe/Mn plaque of *Aegiceras corniculatum* (L.) Blanco seedlings exposed to cadmium. Environ. Nanotechnol. Monitor. Manag. 4, 6–11. https://doi.org/10.1016/j.enmm.2015.04.001

Zhang, Z., Shi, W., Ma, H., Zhou, B., Li, H., Lü, C., He, J., 2020. Binding mechanism between fulvic acid and heavy metals: integrated interpretation of binding experiments, fraction characterizations, and models. Water Air Soil Pollut. 231,184. https://doi.org/10.1007/s11270-020-04558-2

Zhao, F., Ma, Y., Zhu, Y.G., Tang, Z., Mcgrath, S.P., 2015. Soil contamination in China, current status and mitigation strategies. Environ. Sci. Technol. 49 (2), 750–759. https://doi.org/10.1021/es5047099

# Speciation and distribution of chromium (Cr) in rice root tip and mature zone: the importance and impact of root exudation and iron plaque in Cr bioavailability

**Peiman Zandi[a#,b], Xing Xia[a#], Jianjun Yang[a*], Jin Liu[c], Remusat Laurent[d], Cornelia Rumpel[e], Elke Bloem[f], Beata Barabasz Krasny[g], Ewald Schnug[h]**

[a] Institute of Environment and Sustainable Development in Agriculture, Chinese Academy of Agricultural Science, Beijing 100081, P. R. China

[b] International Faculty of Applied Technology, Yibin University, Yibin 644000, China

[c] College of Agronomy and Biotechnology, China Agricultural University, Beijing 100094, China

[d] Muséum National d'Histoire Naturelle, Institut de Minéralogie, Physique des Matériaux et Cosmochimie, CNRS UMR 7590, Sorbonne Université, 75005 Paris, France

[e] CNRS, Institute of Ecology and Environmental Sciences of Paris, IEES, UMR (CNRS-INRA-UPMC-UPEC-IRD), Thiverval-Grignon, 78850, France

[f] Julius Kühn-Institut, Federal Research Centre for Cultivated Plants, Institute for Crop and Soil Sciences, Bundesallee 69, 38116 Braunschweig, Germany

[g] Institute of Biology, Pedagogical University of Krakow, Podchorążych 2 St., 30-084 Kraków, Poland

[h] Institute for Plant Biology, Department of Life Sciences, Technical University of Braunschweig, 38106 Braunschweig, Germany

[#]Xing Xia and Peiman Zandi equally contributed to this work.

* Corresponding author.

E-mail address: yangjianjun@caas.cn; yangjianjun-caas@outlook.com (J. Yang)

# Speciation and distribution of chromium (Cr) in rice root tip and mature zone: the importance and impact of root exudation and iron plaque in Cr bioavailability


## Abstract

Evidence on the contribution of root regions with varied maturity levels in iron plaque (IP) formation and root exudation of metabolites and their consequences for uptake and bioavailability of chromium (Cr) remains unknown. Therefore, we applied combined nanoscale secondary ion mass spectrometry (NanoSIMS) and synchrotron-based techniques, micro-X-ray fluorescence (µ-XRF) and micro-X-ray absorption near-edge structure (µ-XANES) to examine the speciation and localisation of Cr and the distribution of (micro-) nutrients in rice root tip and mature region. µ-XRF mapping revealed that the distribution of Cr and (micro-) nutrients varied between root regions. Cr K-edge XANES analysis at Cr hotspots attributed the dominant speciation of Cr in outer (epidermal and sub-epidermal) cell layers of the root tips and mature root to Cr(III)-FA (fulvic acid-like anions) (58-64%) and Cr(III)-Fh (amorphous ferrihydrite) (83-87%) complexes, respectively. The co-occurrence of a high proportion of Cr(III)-FA species and strong co-location signals of $^{52}Cr^{16}O$ and $^{13}C^{14}N$ in the mature root epidermis relative to the sub-epidermis indicated an association of Cr with active root surfaces, where the dissolution of IP and release of their associated Cr are likely subject to the mediation of organic anions. The results of NanoSIMS (poor $^{52}Cr^{16}O$ and $^{13}C^{14}N$ signals), dissolution (no IP dissolution) and µ-XANES (64% in sub-epidermis >58% in the epidermis for Cr(III)-FA species) analyses of root tips may be indicative of the possible re-uptake of Cr by this region. The results of this research work highlight the significance of IP and organic anions in rice root systems on the bioavailability and dynamics of Cr.



**Keywords:** Cr-speciation, Iron-plaque dissolution, NanoSIMS analysis, phytometabolites, root morphology


## Environmental Implications

Considering how different root regions with varied iron plaque presence, dissolution rate, and diverse root metabolites and their exudations may affect the fate of Cr uptake and bioavailability in rice plants, the present study has, for the first time, set the stage for holistic investigation of two critical parts of the root (tip/mature root) system at a molecular level using combined NanoSIMS and synchrotron-based (μ-XRF/ μ-XANES) techniques. The findings of this study appear to be significant for current and future studies on suppressing heavy metal bioavailability in contaminated paddy soil systems.

## 1. Introduction

Soil contamination with heavy metals, especially chromium (Cr), is a widespread problem that poses threats to human health risks through the food chain (Yang et al., 2019a; Ali et al., 2022). In China, Cr is one of the eight heavy metals most strongly affecting agricultural soils, with a contamination rate exceeding 1.1% (Zhao et al., 2015). Based on the China National Food Hygiene Standard (GB 2762-2017), the bioaccessibility of Cr in rice grain should not exceed the Cr threshold value of 1.0 $mg{\cdot}kg^{-1}$ (Geng et al., 2020; Ali et al., 2022) to avoid adverse health complications (e.g., oxidative stress and DNA damage) associated with dietary Cr intake (Nickens et al., 2010; Khan et al., 2012). Therefore, controlling Cr transfer in the soil-rice system is crucial for food safety.

Root uptake in rice is considered to be the major entry route of soil Cr into edible rice grains. The root system of rice plants consists of seminal, nodal (primary), and lateral roots (Gu et al., 2017). Among them, primary roots are classified into root tips and mature root regions according to the level of development (Seyferth et al., 2010; Zandi et al., 2022). Root tips have underdeveloped vascular systems, lacking the complete formation of the aerenchyma and Casparian bands (CBs). They account only for a small fraction of the overall mineral element uptake in rice plants, while mature rice roots have a fully developed anatomical structure with the cortex (exodermis, aerenchyma, endodermis) and stele (xylem) that support the influx and transport of mineral nutrients (Yamaji and Ma, 2007; Coudert et al., 2010; Fukao et al., 2019).

Similarly to many aquatic or semi-aquatic plants, rice is a hydrophyte species grown in flooded paddy fields. Rice has to cope with anaerobic conditions by radial oxygen diffusion from the root aerenchyma towards the root surface and adjacent rhizosphere (Deng et al., 2010; Xu et al., 2018), where it mediates iron oxidation [Fe (II) to Fe (III)] and development of an amorphous coating of iron (hydr)oxides (known as iron plaque, IP) on the root surface (Cheng et al., 2014; Tripathi et al., 2014; Zandi et al., 2022). Moreover, continuous flooding was indicated to create a favourable rhizosphere environment for IP formation (Xiao et al., 2021). The physical barrier of IP has been proposed to serve as a natural protection mechanism against excess heavy metal concentration in plant parts (Khan et al., 2016).

There is consensus that root capacity for aerobic respiration is the main factor in the oxidising power of the rhizoplane zone (Wu et al., 2012; Holzschuh et al., 2014), and consequently the degree of IP formation (Zandi et al., 2022). Rice root tips with no discernible aerenchyma structures were found to have a higher oxygen discharge in comparison to the basal part of the root (Nishiuchi et al., 2012). Nonetheless, IP was shown to be less frequent around the root tips (Williams et al., 2014) due to their rapid development (Nishiuchi et al., 2012), possibly affecting heavy metal speciation and mobility in this region compared to the basal root region.

Many studies concerning the whole root system have shown that iron (hydr)oxides have a strong binding affinity for metal(loid) ions on the root surface and reduce their mobility and bioavailability, thereby inhibiting the uptake and transport of toxic metals, including Cr (Hu et al., 2014; Cao et al., 2018; Zandi et al., 2022). Previous studies have shown that in the absence or weak presence of IP, higher concentrations of Cr were accumulated in root cells rather than in shoots of rice (Xu et al., 2018; Zandi et al., 2020, 2021), suggesting that Cr mainly deposited in root cell walls hindered its transport to the aerial organs (Zeng et al., 2011). The hydroponic and soil culture experiments have demonstrated that an appropriate amount of IP on root surfaces could effectively adsorb Cr(III) and Cr(VI) species and reduce their transfer to the rice roots and shoots, thus decreasing Cr concentrations in rice tissues (Xu et al., 2018; Yu et al., 2017; Zandi et al., 2020).

In addition to the inhibition of iron (hydr)oxides, other factors such as root exudates, which mainly consist of low or fairly low molecular weight (LMW) organic anion metabolites, with various

chemical functional groups (e.g., –COOH, –OH) (Seal et al., 2004), have been proposed to interact with iron (hydr)oxides during sorption and chelation of heavy metals in the soil (Zhang et al., 2020) and plant systems (Wang et al., 2019). Moreover, earlier studies have shown that these metabolites can enhance the dissolution of iron (hydr)oxides bound to heavy metals, leading to their release into the rhizosphere (Sebastian and Prasad, 2016; Luo et al., 2017; Saad et al., 2017). Studies on the entire root system in environments contaminated with cadmium (Cd), aluminium (Al) and Cr have indicated that organic anion secretions are highly associated with increased heavy metal tolerance through their efflux into the rhizosphere (Yang et al., 2013; Saad et al., 2017; Yang et al., 2019b; Bali et al., 2020). This efficient exclusion mechanism reduces metal uptake and accumulation in plants (Montiel-Rozas et al., 2016).

In the rice root system, these metabolites may also act as a defensive barrier for the roots by forming stable complexes with Cr (Uren, 2000; Zeng et al., 2008) or affecting their reduction and immobilisation in the root (Xiao et al., 2023). Therefore, the contribution of root exudates to increased Cr accumulation in rice roots could be related to the tolerance mechanism through chelation (Hayat et al., 2012; Agnello et al., 2014). The rate and composition of metabolites released in response to Cr stress correlate with plant genotype (Zeng et al., 2008) and metal speciation of Cr (Pradas del Real et al., 2014).

Previous studies on the importance of IP or root exudation in suppressing the bioavailability of heavy metal Cr in rice plants mainly focused on the evaluation of the entire root system (Zandi et al., 2020; Xiao et al., 2023). This study has addressed for the first time how individual root regions with varied maturity levels (e.g., less developed tips) may differ in the degree of IP formation or in the secretion of organic anions in response to Cr stress. Further, the issues concerning the correlation of these secretions with IP dissolution and Cr release, and whether IP dissolution mediated by root metabolites can alter Cr mobility and bioavailability have also been analysed. Moreover, it remains unclear whether the main root regions vary in their contribution to Cr chelation and immobilisation, and reduced Cr accumulation in tissues under the influence of iron plaque and root exudation.

To bridge the gap, the present study explicitly proposed the combined application of state-of-the-art high-sensitivity ion mass spectrometry (NanoSIMS) and synchrotron-based microprobe techniques,

such as micro-X-ray absorption near-edge structure spectroscopy (μ-XANES) and micro-beam X-ray fluorescence (μ–XRF), to investigate the distribution and/or speciation of elements of interest (X) in different root regions (root tips/ mature root) of rice at submicro- and microspatial scales, and their association with $^{13}$C-labelled root exudates on the active root surface.

The objectives of this study were to (1) explain/assess the interaction between Cr and Fe and its effect on Cr uptake and translocation in rice plants, (2) elucidate the molecular speciation of Cr and binding mechanisms of Cr species in different root regions, and (3) to localise the active root surface with exudate release and its impact on Cr uptake by different root regions. We expected that these results would provide a theoretical basis for understanding heavy metal sequestration and dynamics on iron plaques and their benefits to human health by reducing rice contamination. We expected that these results would provide a theoretical basis for understanding heavy metal sequestration and dynamics on iron plaques and their benefit to human health by reducing rice contamination.

## 2. Materials and methods

### 2.1. Plant culture, treatments and metal extraction

Rice seed (*Oryza sativa* L. Var. Xiangzaoxian 31) germination (7 days on moist gauze in plastic Petri dishes in the dark at 28°C) and initial growth (21 days in black plastic containers) were conducted under controlled sterile conditions in half-strength nutrient solution (Table Supplementary (S) 1-S1), as previously described (Zandi et al., 2021). The variety was a high-quality, early-maturing, hybrid-based (Chen et al., 2000; Yu, 2018) model crop for bioremediation studies used at the Institute of Environment and Sustainable Development in Agriculture, Chinese Academy of Agricultural Sciences in Beijing.

The seedlings of the first group, intended for iron plaque (IP) formation (Fe80-CK; Fig. S1), were transferred to solutions spiked with 80 mg $L^{-1}$ ferrous iron ($FeSO_4 \cdot 7H_2O$), incubated for 24 h and subsequently transferred into quarter strength and total strength nutrient solution for 2 and 3 days, respectively. The second group (Fe0-Cr(III)) was not subjected to IP induction, but was grown in a nutrient solution containing 1.0 mg $L^{-1}$ $CrCl_3 \cdot 6H_2O$ for 3 days, and then transferred to a quarter-

strength nutrient solution for 2 days. The first two groups were exclusively designed for bioavailability analysis and were not included in the follow-up investigations described in sections 2.2, 2.3 and 2.4. The third group (Fe80-Cr(III)) was a combination of the two aforementioned treatments, where seedlings with IP were exposed to Cr(III)-spiked solutions for 3 days. Each treatment was performed in three replicates. Replenishment of depleted nutrients in culture solutions was carried out every three days, and manual adjustment of the solutions to a suitable pH of 5.5 was done using 0.1 M HCl and NaOH (Zandi et al., 2020). All seedlings were grown in a controlled plant growth chamber (PGX-350D, NSEI Co., Ltd., China) with a relative humidity of 70% dedicated to predetermined periodic dark (10 h, 20 °C ) and light (14 h, 28 °C, 300-350 µmol $m^{-2}s^{-1}$) regimes. The selected Fe and Cr concentrations were based on recommendations and results of earlier studies (Hu e al. 2014; Li et al., 2015; Yu et al., 2017; Zandi et al., 2020).

The seedlings were collected, split into roots and shoots and rinsed with deionised water. Fresh roots with IP were initially divided into the tip (from the root cap to the zone without root hair; ~2-3 cm) and mature (from the root hair zone to the base of primary roots) sections, and subsequently incubated for 30 min at room temperature (25°C) in 30 mL of cold DCB (dithionite–citrate–bicarbonate) solution containing $NaHCO_3$ (0.125 M), $Na_3C_6H_5O_7$ (0.03 M) and $Na_2S_2O_4$ (0.5 g) (Liu et al., 2004). After incubation, the sections were thoroughly washed with deionised water and removed from incubation tubes. The remaining extracts were initially filled up with deionised water to a volume of 50 mL and subsequently passed through a 0.45-µm filter to remove root debris.

The digestion of plant materials was carried out according to Hu et al. (2014) with some modifications. Briefly, plaque-free root sections were oven-dried (similar to shoot samples) and homogenised, pre-digested overnight in heat-proof tubes (100 mL) in 5 mL of concentrated $HNO_3$ (~65-68%). Digestion was completed in a digester heating block at 160°C for ~3 h and after cooling to room temperature, diluted in 25 mL of deionised water and filtered. A reagent blank and a series of external standard solutions (e.g., GBW07605) from certified reference materials in China were utilised to validate the quality control and accuracy of the entire digestion procedure. Fe and Cr contents in the digestion solutions and DCB extracts were quantified using ICP-OES (Agilent 5110, Agilent Technologies, Inc., USA).

## 2.2. Synchrotron-based microprobe analysis

Freshly sectioned root specimens were stored at –30°C until synchrotron-based microprobe analyses. For μ-XRF imaging of root surfaces using the VESPERS beamline at the Canadian Light Source (CLS), the roots were sectioned and flatly fixed on a Kapton tape. For μ-XRF/μ-XANES analyses of root cross sections using the 15U beamline at the Shanghai Synchrotron Radiation Facility (SSRF, Shanghai), the corresponding root sections were cut into 60-μm-thick slices by a microtome, and subsequently mounted onto a Kapton tape for freeze-drying and stored at –20°C (Tian et al., 2010; Lu et al., 2017). As described in previous studies (Yang et al., 2015; Wang et al., 2021), the μ-XRF method of both beamlines was similar, except that the data in VESPERS were analysed using SMRK software, thus here we have only reported the experimental details for the 15U beamline at the SSRF.

X-rays with an incident energy of 10 keV were monochromatised using a Si (111) double-crystal monochromator. The spot size of the X-ray beam was micro-focused to 10 μm x 5 μm using a Kirkpatrick-Baez (K-B) mirror system for scanning. The root samples were placed at an angle of 45° to the beam incidence perpendicular to a 7-element Si(Li) detector (e2v, USA). After selecting the region of interest by the microscope, the region was scanned step by step by moving the sample stage with a step size of 5 and 10 μm for x and y direction, respectively. First, the whole fluorescence spectrum was acquired, and then the fluorescence signals of the elements of interest, including K (3.3 keV), Ca (3.6 keV), Cr (5.4 keV), Mn (5.9 keV), Fe (6.4 keV) were selected and applied to all pixel spectra to obtain multi-elemental 2D mapping with a dwell time of 1.5 s per pixel. After analysing the μ-XRF images using Igor Pro 6.0 software (IGOR), the spots of interest were selected for Cr K-edge μ-XANES spectra collection in the fluorescence mode at 25°C. The energy range and step were set to 5931-6080 eV and 0.5 eV, respectively. Several scans were collected from each spot and later averaged to obtain a merged spectrum with a better signal-to-noise ratio. At least 2 hotspots from cross-sections of the root tips and mature root regions were considered for μ-XANES spectrum collection. Cr foil was also used to calibrate the beamline (X-ray) energy.

Cr K edge μ-XANES spectra of Cr(III) adsorbed on ferrihydrite (Cr(III)-Fh) and organo-Cr(III) complexes (Cr(III)-FA) (synthesised by the interaction of $CrCl_3$ with fulvic acid) (Yang et al., 2020) were acquired in the fluorescence mode and Cr(III) acetate in the total electron yield mode, and were

referred to as Cr reference standards. Since root iron plaques induced in a short 24-h period were poorly crystallised and mostly amorphous (Xu and Yu, 2013), ferrihydrite, a typical amorphous iron (hydr)oxide formed during iron hydrolysis (Yang et al., 2020), was considered as the principal sorbent for Cr (III) sequestration in rice root IP in this study. Athena software (Ver. 2.1.1) was used for fingerprint and linear combination fitting (LCF) analysis of sample μ-XANES spectra (Ravel and Newville, 2005). Cr speciation and the percentage of each Cr species were determined based on the LCF of Cr K-edge μ-XANES spectra of the hotspots using the spectra of the reference compounds as end-members (Peng et al., 2015). The goodness of data fitting was assessed using the R-factor.

It should be noted that the limited root samples (one sample/ root section) and spots (2 hotspots/ root cross-sections) measured during the μ-XRF and μ-XANES analyses may not be representative of the whole root samples. However, earlier studies used a similar method and have demonstrated that the output result could account for most of the sample variation (Lombi and Susini, 2009; Seyfferth et al., 2010; Frommer et al., 2011; Li et al., 2015; Yang et al., 2015).

### 2.3. $^{13}CO_2$ labelling of rice and NanoSIMS analysis

The procedure for uniform $^{13}CO_2$ labelling of rice was as described earlier (Ge et al., 2012; Yuan et al., 2016) with some modifications. Briefly, rice seedlings belonging to the third treatment group (Fe80-Cr (III)) were first exposed to $CrCl_3$ treatment for 24 h and subsequently transferred to normal (Cr-free) nutrient solution and kept in transparent airtight perspex $^{13}CO_2$-labelling and non-labelling control boxes (40 cm long × 50 cm wide × 60 cm high; Fig. S2) for 24 h. During this period, the concentration of $^{13}CO_2$ inside the labelling box atmosphere was maintained at approximately 400 μL $L^{-1}$ (ppm) by controlled injection of 0.1 M $Na_2{}^{13}CO_3$ solution ($^{13}C$-enriched > 99%) into 1 M HCl solution. A $CO_2$ detector spectrometer (IRMS, RS-CO2WS-N01-2, Shandong Renke Control Technol. Co., Ltd., China) was used to monitor $CO_2$ concentration inside the labelling boxes (Kaiser et al., 2015). Isotopic labelling of rice seedlings with $^{13}C$ was performed by photosynthetic fixation of $^{13}CO_2$ in the aforementioned labelling boxes. Seedlings incubated in unlabelled control boxes served as the reference factor for excess $^{13}C$ in shoots and roots after DCB extraction. The environmental growth conditions in the perspex boxes were identical to those described in section 2.1.

Rice seedlings were harvested and separated into roots and shoots before IP dissolution could occur, e.g., as a result of the secretion of $^{13}C$-labelled and/or unlabelled metabolites by the roots. Afterwards, root and shoot samples from both labelled and unlabelled control seedlings were ground to determine $^{13}C$ abundance in the respective plant samples using a C/N element analyser coupled to an isotope ratio mass spectrometer to verify successful labelling with $^{13}C$ (Isoprime 100, Elementar's PYE cube, UK). Freshly sectioned root specimens were immersed in a tissue freezing medium (SAKURA Tissue-Tek OCT) for rapid freezing at −30°C. Root sections were then axially frozen-cut into 60-µm-thick slices using a microtome (Reichert-Jung, Germany). The slices were collected and mounted onto a $Si_3N_4$ wafer and coated with gold (20 nm thick) for NanoSIMS analysis.

Cross-sections of mature roots and root tips were imaged using Cameca NanoSIMS 50 installed at the Museum National d'Histoire Naturelle, Paris, France. The surfaces of the root samples were scanned with a 16 keV $Cs^+$ (caesium) primary beam, set to 1 pA, leading to a spatial resolution of approximately 150 nm. Secondary ions were collected in multicollection mode: $^{12}C^-$, $^{16}O^-$, $^{12}C^{14}N^-$ and $^{13}C^{14}N^-$ in the first run (for C isotope and N/C mapping), and $^{16}O^-$, $^{12}C^{14}N^-$, $^{13}C^{14}N^-$, $^{52}Cr^{16}O^-$ and $^{56}Fe^{16}O^-$ in the second run (to determine associations of organic matter and heavy metals). Image processing and data analysis were carried out using the freeware package OpenMIMS (multi-isotope imaging mass spectrometry, freely available at http://nrims.harvard.edu). In total, more than eight NanoSIMS images were acquired from the labelled samples. More detailed information on $^{13}C$ isotopic maps and NanoSIMS image processing are provided in Supporting Information (SI)-A.

2.4.Fe plaque dissolution experiment

The function of root exudates in the dissolution of iron (hydr)oxides and release of their associated Cr into the medium was investigated in a time-lapse experiment. To this end, another set of plaque-bearing rice seedlings was exposed to Cr treatment (Fe80 × Cr(III)) and allowed to grow in the same nutrient solution for another 16 days. The sampling schedule was established for days 1, 3, 7, 10 and 16. Root samples at each sampling stage were subjected to DCB extraction for ICP readings of Fe, Cr and calcium (Ca).

### 2.5.Data analysis and statistics

All Cr-based computations were based on previously described equations (Liu et al., 2004; Zandi et al., 2020). The R statistical package (ver. 2.12.1) was used for all statistical analyses, and statistical differences between treatment means were assessed using the least significant difference (LSD) test at the 0.05 probability level (Data presented here are means ± SD, n=3).

## 3. Results

### 3.1.Fe and Cr concentrations in different root regions

Regardless of the examined root regions, the quantities of Fe and Cr adsorbed on IP (DCB extracts) in the roots treated with Cr were significantly higher than in the non-treated roots ($p < 0.05$) (Fig.1a,b). The observed discrepancies between Cr concentrations in DCB solutions extracted from different root sections were statistically significant ($p < 0.05$; DCB-Cr in mature root > root tip). Similarly, Cr concentrations in root tissues were in the following order: Root-Cr mature > Root-Cr tip ($p < 0.05$) (Fig.1b). Seedlings treated with Cr (+Cr seedlings) had higher Fe and Cr contents in their root tissues compared to non-treated counterparts, with markedly increased Fe accumulation in both the tip (2.25-fold) and mature root (1.72-fold) sections. It was also found that the overall Fe sequestration in IP (DCB-Fe) on the mature root surface was significantly higher compared to the tip region both under stress (Fe80-Cr(III)) and stress-free (Fe80-CK) conditions. Fe content in the root tip was significantly higher than in the mature root under Cr stress conditions (Fig.1a).

### 3.2. Fe and Cr concentrations/proportions in different rice parts

The respective concentrations of Cr and Fe in shoots, plaque-free roots, and DCB extracts differed in their distribution pattern. While the concentration (or relative proportion) of Cr in roots (53%) was significantly higher than that accumulated in IP (~37%) and shoots (~10%), the relative concentration of Fe in individual rice components was in the following order: DCB-extractable Fe > Root-Fe > Shoot-Fe (Table 1). Fe mainly accumulated in IP on the root surface under both stress (~89%) and stress-free (~91%) conditions. Irrespective of Cr levels applied, Fe concentration in

shoots did not show any significant differences, whereas Fe concentration in IP and roots of Cr-treated seedlings (Fe80-Cr(III)) was significantly (~1.52 to 1.98 times, respectively; $p$ <0.05) higher compared to non-Cr treated seedlings (Fe80-CK) (Table 1; Fig. S5a). Only 1.5% of the total Cr contents in roots translocated to shoots, with an 8.8% root-to-shoot Fe translocation efficiency observed in rice exposed to Cr treatment (Table 1).

### 3.3. Elemental distribution in rice root

#### *3.3.1.Two-dimensional surface view of the root tip and mature root sections*

The results of *in vivo* scanning of Fe and Cr deposits on the epidermal surface of the root tip (Fig. 2$a_{1-2}$) and mature root (Fig. 2$a_{4-5}$) sections were partially consistent with ICP-OES analyses concerning elemental distribution (Fig.1). The distribution patterns of Fe, Cr, and Ca fluorescence signals in the root tips after Fe80-Cr(III) treatment were relatively weak (low-intensity spots), with their hotspots scattered and located in slightly distant positions (Fig. 2$a_{4-6}$). Such distribution of elemental intensities was considerably different from that observed in the mature section of the root, where the intensity of elemental distribution mostly ranged from moderate (green), upper-moderate (yellow) to high (red) levels.

According to the results of correlation analysis, the element Cr showed a slightly low ($R^2$= 0.57) to rather high ($R^2$= 0.77) associations with high Fe intensities (~45-80 kilo-counts $s^{-1}$) and a range of low to moderate associations with Ca (~0.2-2.3 kilo-counts $s^{-1}$) intensities, respectively, in IP deposited in the tip zone of rice roots (Fig. 2$b_{4-5}$). Ca distribution pattern appeared to be similar to that of Fe in the mature root zone, signifying a strong linear association between Fe (~ 5-55 kilo-counts $s^{-1}$) and Ca (~ 0.15-25 kilo-counts $s^{-1}$) concentration intensities ($R^2$= 0.90; Fig. 2$b_3$). Similarly, Cr concentration was the highest in the mature root zone (Fig. 2$a_1$), and greatly co-localised with Ca ($R^2$= 0.91) and Fe ($R^2$= 0.90) intensities observed in the same root zone (Fig. 2$b_{1-2}$). The majority of Cr deposits in the mature zone of rice root was strongly correlated with a wide range of moderate (>50 kilo-counts $s^{-1}$) to high Fe intensities (<550 kilo-counts $s^{-1}$). Therefore, Cr was suggested to have a strong association with Fe concentration intensities in the mature zone of rice roots, and this mostly occurred in the Cr intensity range of ~10-38 kilo-counts $s^{-1}$ (Fig. 2$b_1$).

For Cr signals emitted from the upper surface of the root tip and mature root sections, several hotspots of moderate to high intensity were found, which were thought to be related to significant fractions of Cr sequestered in IP. As outlined above, the concentrations of Cr, Fe and Ca tended to be more intense in the mature root zone than in root tips. The majority of low to high Cr counts (~1.3 to 32.5 kilo-counts $s^{-1}$) correlated mostly with a low to moderate (~0.2-2.6 kilo-counts $s^{-1}$) counts of Ca intensities in the tip zone of rice roots after Cr treatment (Fig. 2$b_5$). Ca was mainly distributed on the epidermal surface of the mature root zone and this signal was reproduced by the element Fe. The lower correlation of Cr with Fe (Fig. 2$b_4$) to Ca (Fig. 2$b_5$) could also be attributed to the co-distribution of these two elements at hotspots, with no apparent correlation (or overlap) in their moderate-intensity spots. The result indicated that the correlation between the intensities of Fe and Ca fluorescence counts in root tips ($R^2$= 0.37) was considerably lower than that in mature roots ($R^2$= 0.90) under Fe80-Cr(III) treatment (Fig. 2$b_{3-6}$). The low correlation between Fe and Ca counts in root tips could be explained by a partial overlap of Fe hotspots in root tips in regions where Ca fluorescence intensity was high.

*3.3.2.Two-dimensional cross-section views of the root tip and mature root tissues*

Cr was mainly localised in the epidermal and exodermal layers of both rice root sections. A higher concentration of Cr was observed in the internal portion of sclerenchyma cells in the root tips in comparison to the mature root section (Fig. 3$a_{1-2}$). In other words, Cr was enriched (with more noticeable Cr spots) in the outer epidermis of mature roots. As shown in Fig. 3$b_1$, high-intensity Fe spots could be observed on the most distal sides of epidermal and exodermal cells, while moderate-intensity Fe spots were dispersed in sclerenchyma cells. In contrast, the inner portions of the exodermal layer in the tip section showed a higher Fe content than the epidermis (Fig. 3$b_2$). Moreover, Fe distribution was visible in root tip vessels, which likely corresponded to the vascular tissues of the root, implying that Fe could penetrate the root tip surface into the stele and move upward. However, there was no clear signal of Fe presence in the inner tissues of the mature root zone. Higher Fe concentrations were recorded on the epidermal surface of the mature root zone, as opposed to the root

tip zone after Fe80-Cr(III) treatment. This result was consistent with our root surface μ-XRF analysis, where an Fe-enrichment zone was observed on the dorsal surface of the mature root zone.

The co-occurrence of Fe and Cr in the epidermal and sclerenchyma cells was found in both root regions (Fig. 3$a_{1\text{-}2}$, $b_{1\text{-}2}$). The correlation of Fe and Cr deposition was more pronounced in the mature zone than the root tip zone, where, unlike the moderate amounts of Fe present in the root stele, no Cr was located in this region (Fig. S3). It can be suggested based on the overlapping Fe and Cr signals that there was a close correlation between Cr and Fe deposits in the epidermal and exodermal cell layers in both sections of rice roots.

Fig. 3$c_{1\text{-}2}$ illustrates the effect of Cr on S distribution in the root tip and mature root cross-sections. It is shown in Fig. 3$c_1$ that S was mainly dispersed in the outer cell layers (along the epidermis and exodermis), in the ground tissues (across the cortex and endodermis) and the stele (pericycle and vascular bundles) of the rice root. With the exception of the middle and central tissues, moderate-intensity S spots in the epidermis and exodermis layers correlated well with Fe hotspots (Fig. 3$b_{1\text{-}2}$; not marked), followed by Cr moderate-intensity spots. In comparison to Fig. 3$c_1$, a significant decrease in S accumulation was found across the epidermis and exodermis tissues of rice root tips (Fig. 3$c_2$). However, S distribution in the endodermis, pericycle, and stele of root tips was more extensive than in the mature root zone. This suggested that a considerable proportion of S could penetrate the stele in both sections of rice roots. Fig. 3$a_2$,$b_2$,$c_2$ demonstrated that S distribution did not follow the pattern observed for Fe and Cr in the outer cell layers of the root tip cross-section.

Potassium (K) and Ca primarily accumulated in the internal cell layers of both root sections, including endodermis, pericycle and vascular cylinder, as determined by high K and Ca fluorescence intensities (Fig. 3$e_{1\text{-}2}$,$f_{1\text{-}2}$). This observation suggested successful penetration of both elements into the root xylem and their subsequent possible translocation to the shoot. Images $e_1$,$f_1$ and $e_2$,$f_2$ in Fig. 3 clearly demonstrated that the cortex tissue in the mature root of Cr-exposed rice contained a limited degree of an irregular radial dispersion/gradient of K and Ca relative to the root tip zone. This result suggested that K and Ca tended to accumulate in vascular tissues. The distribution pattern of K was analogous to that of Ca in rice roots from both regions. Regardless of the Mn-free region in the cortex and Mn-enriched region in the stele, Mn concentration in the outer cell layers approximately

resembled Cr concentration in the rice root maturation region (Fig. 3$a_1$,$d_1$). Mn distribution in the rice root tip region was not only limited to the outer cell layers and stele, but also included parts of cortical tissues (Fig. 3$d_2$).

### 3.4. Cr K-edge μ-XANES analysis

One main peak and two shoulders, resolved at ~5999.0 eV (peak- 1), ~6005.0 eV (shoulder- 2) and ~6015.0 eV (shoulder- 3), respectively, were recorded in the Cr K-edge XANES spectra associated with spots of interest (SOIs) in the mature and tip region of the root (Fig. 4a). These features were more similar to Cr(III)-Fh and Cr(III)-FA standards rather than the Cr(III) acetate standards with a broader peak 1. The first derivative spectrum of Cr(III) acetate showed an apparently lower energy position of peak b compared to other standards and samples (Fig. 4b). In addition, peak b for all hotspot first derivative spectra displayed a similar shape to Cr(III)-Fh. However, peak c, which appeared in the first derivative spectra of Cr(III)-FA and all hotspots, was absent in Cr(III)-Fh. Therefore, Cr could co-exist and/or form complexes with fulvic acid-like (~FA) substances as an organic metabolite with more diverse functional groups (Qin et al., 2016; Wang et al., 2019; Zhang et al., 2020) and/or ferrihydrite as a typical amorphous form of iron (hydr)oxide in the outer cell layers of rice roots (Tripathi et al., 2014; Zandi et al., 2020).

LCF analysis based on spectral features (Fig. 4a) revealed that Cr(III) bound to FA-like anions accounted for 58-64% (spot 2-spot 1) and 13-17% (spot 2-spot 1) of total Cr in the tip and mature regions of rice roots, respectively (Fig. 4c). In other words, the epidermal layer (spot 1) of the mature root and the sub-epidermal layer (spot 1) in the root tip contained the highest proportion of Cr(III)-FA species compared to spot 2 in the corresponding layers. The outer cell layers of the root tip (spot 1 and spot 2) contained mainly Cr(III)-FA species, whereas Cr was mainly present as Fh-bound Cr(III) in the IP of the mature root outer cell layers (83-87% of total Cr). This result suggested that the immobilisation of Cr through complexation with ferrihydrite in IP on the outer cell layers of the mature root was more important than the immobilisation of Cr species by complexation with phyto-/organic metabolite compounds. More than 83% of total Cr was present as Cr(III)-Fh species in spot 1

and spot 2 of the mature root zone, which was considerably higher compared to spot 1 and spot 2 of the root tip zone.

### 3.5. Carbon isotope results

The mean $\delta^{13}C$ values showed a remarkable disparity between the plaque-free $^{13}C$-labelled (515.04‰) and non-labelled (-30.00‰) root samples (Table S2), indicating that the downward flux of photosynthetically processed $^{13}CO_2$ was significant (successful $^{13}C$ labelling) during the short period of our experiment. However, in terms of C concentrations in labelled/non-labelled roots, this discrepancy was not that robust since ~1.1% $^{13}C$ in the C pool of the non-labelled root samples was partially similar to ~1.7% $^{13}C$ in the C pool of the $^{13}C$-labelled roots. The results demonstrated that plants with IP on their roots tended to assimilate less $^{13}C$ out of $^{13}CO_2$ than plants devoid of plaque. We therefore found small differences between the $^{13}C$ abundance values in $^{13}C$-enriched root cells with or without IP induction. The severe reduction in C mass percentage (C%) in plaque-bearing roots compared to plaque-free roots was likely caused by the contribution of Fe (III) precipitates to the mass balance disturbance, regardless of whether roots were labelled or not.

The labelled shoot samples had a 3 times higher $^{13}C/^{12}C$ ratio (and $^{13}C$ abundance) compared to the non-labelled shoot samples. It should be noted that the existing differences in $\delta^{13}C$ and $^{13}C$ abundance between the labelled root and shoot samples did not significantly affect the mass percentage of C in the corresponding samples. In comparison with shoot tissues, root tissue (with or without IP) samples exposed to isotopically labelled $^{13}CO_2$ showed a lower proportion of $^{13}C$ isotope abundance, ranging from 49.9% to 51.9%. Another noteworthy aspect to consider was whether the presence of IP on the root surface altered C content in $^{13}C$-labelled roots. In this regards, our results demonstrated a substantial decrease (to about 49%) in C content of the plaque-bearing roots (Fe$^{13}C$-root) compared to plaque-free roots ($^{13}C$-root). It was assumed that the observed differences between the above samples could be associated with the release of metabolites into the culture medium, or even their lower production in the aerial parts, and thus decreased metabolic activity when IP was present.

### 3.6. Distribution mapping of metals and $^{13}C$ by NanoSIMS

NanoSIMS was used to map the relationship between metabolically active $^{13}C$-enriched root epidermal cells and metal complexes such as CrO and FeO (hereinafter referred to as iron (oxy) hydroxide mineral) in both the tip and mature root regions. Two selected areas of root tips (Fig. 5b) and mature roots (Fig. 5a) were analysed and colour composite images specifically showed the epidermal cell layer of the roots treated with ferrous-spiked solutions and Cr(III). Regions of interest in the two sections were defined based on whether iron (oxy) hydroxide minerals were present on (or within) the epidermal cell membrane. Comparison of the tip with the mature region allowed for accurate tracking of $^{13}C$-enriched metabolites in these two areas. The presence of $^{13}C$-enriched cells was more abundant in the epidermal cell layers of mature roots than in the root tips (Fig. 5).

Based on composite images showing relative locations of species, such as $^{52}Cr^{16}O$, $^{13}C^{14}N$ and $^{56}Fe^{16}O$, metabolically active epidermal cells in the mature root region were more enriched in $^{13}C$ metabolites compared to the root tip. The location of $^{13}C$-enriched metabolites was confined to the epidermal cell walls (area 1 in Fig. 5a,b) and apoplastic spaces (area 2 in Fig. S4$a_1$). It was also established that $^{13}C$-labelled metabolites in the above-specified spots co-localised with Fe and Cr. Moreover, $^{56}Fe^{16}O$ hotspots were always associated with a somewhat similar accumulation of $^{52}Cr^{16}O$. The $^{56}Fe^{16}O$ signal indicated that Fe was mainly located on the root epidermal surface, irrespective of the root zone. This phenomenon was more pronounced in the mature than in the immature (tip) region of the root, with the outer (excluding epidermis) and inner cell (ground tissues and stele) layers of the latter zone markedly associated with strong $^{56}Fe^{16}O$ signals (Fig. 3$b_2$).

The distribution of $^{56}Fe^{16}O$ in the two studied zones was heterogeneous with distinct regions of accumulation along the outer edge of the root epidermis (area 2 in Fig. 5a,b). The $^{16}O$ images in the two analysed zones clearly demonstrated that O signals were more evident in the mature root zone than in the root tips (Fig. S4). The general pattern of O distribution in $^{16}O$ images resembled the distribution observed in $^{56}Fe^{16}O$ and $^{52}Cr^{16}O$ images. Regardless of the root zone, the strongest $^{56}Fe^{16}O$ and $^{16}O$ signals originating from the outer epidermal cell wall layer were tightly linked with each other, implying that Fe was likely associated with oxide or oxy-hydroxide on the root surface. The presence of overlapping signals of $^{56}Fe^{16}O$ and $^{13}C^{14}N$ or $^{12}C^{14}N$ (organic carbons, OCs) in

specific locations on the root surface suggested the occurrence of organo-Fe oxyhydroxide co-precipitates (OFC) complexes in the examined root regions (SI-B).

### 3.7. Cr release during iron plaque dissolution

The mature root region appeared to have a lower Cr to Ca ratio compared to the root tips, regardless of the sampling time (Fig. 6). This discrepancy was attributed to the higher intensity of Ca distribution on the mature root surface (Fig. 2a$_{3\text{-}6}$). Fluctuations in the Fe/Ca ratios observed in the root tip were not statistically significant ($p > 0.05$), while a significant difference between the Fe/Ca ratios in the mature root zone (initial sharp decrease from day 1 to day 3) was recorded. The decrease in this region was followed by a slight insignificant increase (day 3-day 7) and then another decrease (day 7-day 10). This decline continued for the next 6 days (day 10-day 16). The trends in changes in the Cr/Ca ratios in each of the root sections were identical to those observed for the Fe/Ca ratios, suggesting that the release of immobilised Cr into the medium solution was consistent with IP dissolution.

## 4. Discussion

The results of the present work supported the hypothesis that plant exposure to Cr stress further stimulated $Fe^{2+}$ exclusion and oxidisation on the root surface (i.e., iron (hydr)oxide(s)/ IP formation) due to elevated root oxygen release or enzymatic oxidation (Table 1 ; Fig. S5a) (Briat et al., 2010). This effect was more confined to the mature zone of the rice root surface (Fig. 1a), presumably due to the more developed structure (Nishiuchi et al., 2012). Thus, this region could better limit Cr's bioavailability and mobility than immature root tips (Fig. 1b).

Iron (hydr)oxides serve not only as a physical barrier with a metal-sequestering ability (Amaral et al. (2017) but also as metal-chelating ligands (e.g., DMA: 2′-deoxymugenic acid), which can bind heavy metals (Banakar et al., 2017). This may explain why Fe accumulation in the tip zone was slightly higher than in the mature root zone under Cr stress (Fig. 1a).

Root Cr content was higher than in DCB extracts and shoots (Fig. 1b; Fig. S5b). This suggests that IP formation in conditions similar to flooded cultivation and its inhibitory effect on Cr uptake (Xiao et al., 2021) is not necessarily limited to the root epidermal surface (Fig. $2a_{2\text{-}5}$). This condition most likely involves the apoplastic space in the outer layers of root cells (Fig. $3b_{1\text{-}2}$) (Khan et al., 2016). It appears that Cr-induced increased aerenchyma-rhizosphere oxygen outflux, coinciding with higher Fe concentrations (Fig. $3b_{1\text{-}2}$) (Becker et al., 2020), resulted in an increased amount of Cr precipitated on the outer cell layers compared to internal cell tissues in the tip and mature zone of rice roots (Fig. $3a_{1\text{-}2}$). It's worth noting that increased Cr retention in outer cell layers of plaque-bearing roots compared to plaque-free roots was not associated with aerial uptake (Fig. S5b). This underlines the significance of IP in Cr immobilisation (Zandi et al., 2020, 2021).

The observed correlation between Cr and Ca concentration intensities in surface µ-XRF imaging of overlapping areas (Fig. $2a_{1\text{-}3,}$ $a_{4\text{-}6,}$ $b_{2\text{-}5}$) indicated the importance of Ca as a critical factor in rigidifying cell walls and providing structural integrity to cellular membranes (Hepler, 2005; Pathak et al., 2021) in Cr cell wall sequestration by binding to it (Zeng et al., 2011). This effect was particularly restricted to the outer surface (i.e., epidermal layer) of the mature root zone, where similar Cr (Fig. $2a_1$), Fe (Fig. $2a_2$) and Ca (Fig. $2a_3$) concentration intensities indicated the co-precipitation of Fe with Ca and Cr on epidermal root surfaces. It has been shown by sorption experiments that Ca (Gunnars et al., 2002; van Genuchten et al., 2014) and Cr (Yu et al., 2017) can react with surface hydroxyl groups and adsorb on iron oxides.

In the present study, Cr accumulation in the outer cell layers (except for the epidermis) was not associated with Cr deposition on cell walls (Fig. $3a_{1\text{-}2}$), as indicated by the low correlation between Ca and Cr intensities ($R^2$= 0.01) in both root regions (Fig. S3). In contrast to our finding, in their research on arsenic (As) and Cr (VI), respectively, Xu et al. (2022) and Zeng et al. (2011) attributed the inhibitory role of cell walls to the entire root tissue. This difference might be related to the higher mobility of metal species used in their studies.

The formation of Fe and Mn plaque on rice roots is indeed a ROL (radial oxygen loss)-mediated exclusion strategy for limiting the absorption of potentially toxic elements (Yu et al., 2017; Li et al., 2019). Consistently with Crowder and Coltman (1993), Ye et al. (2001) and Zhang et al. (2015), the

concentration of Fe deposits in the outer cell layers of both root regions in this work was also more intense compared to Mn deposits (Fig. 3$b_{1-2}$,$d_{1-2}$). Therefore, it was not surprising that the co-occurrence of Fe and Cr deposits in hotspot and non-hotspot regions was more pronounced than that of Mn and Cr deposits in both regions of the root (Fig. 3; Fig. S3). It is generally accepted that the functional groups in IP have the potential to form a more active substrate for metal sequestration (Cao et al., 2018; Xu et al., 2018) than those in Mn plaque with its unique catalytic capacity and surface activity (Ye et al., 2001; Liu and Zhu, 2005). In addition to Fe and Mn plaques, sulphur (S) containing metabolites are also effective in Cr chelation and subcellular sequestration (Holland and Avery, 2011; Zandi et al., 2021), as was evident in simultaneous S and Cr depositions in the examined root regions (Fig.3$a_{1-2}$, $c_{1-2}$).

Exclusion and chelation mechanisms seem to co-occur in rice roots during Cr stress exposure, which may lead to decreased Cr entry into the inner layers of root cells and hence lowered Cr uptake, as seen in Fig. 3$a_{1-2}$ and Fig. S5b. This would confirm the hypothesis that root exudation of organic metabolites effectively reduces heavy metal uptake by rice at the root-rhizosphere interface (exclusion strategy) (Wang et al., 2019; Zhang et al., 2020).

The results of the XANES spectra of spots of interest (SOIs) in Cr µ-XRF mapping showed that phytometabolites involved in Cr chelation and detoxification were likely LMW fulvic acid-like (~FA) anions (Fig. 4c) (Wang et al., 2019; Zhang et al., 2020) which have not been reported for soil-free plant systems. These compounds are supposed to form stable chelate compounds with certain heavy metals (chelation strategy), such as Cd (Rashid et al., 2018) and Cr (Pradas del Real et al., 2014), enabling plants to withstand Cr-induced toxicity (Chen et al., 2017). Besides, reports indicated the high affinity of these metabolites for Fe(III) and other structurally similar trivalent metal cations, including Mn (III) (Tang et al., 2010; Saad et al., 2017).

The proportion of Cr(III)-FA complexes varied between individual SOIs (spot 1 and spot 2) in both root regions, proposing two different models (Fig. 4c). On the one hand, a higher percentage of phytometabolites or FA-like anions was bound to Cr(III) species adjacent to the root surface compared to the more internal tissues in the mature root (17% vs 13%), suggesting the existence of a resistance mechanism through exclusion (Osmolovskaya et al., 2018; Bali et al., 2020). On the other hand, a

reverse trend (58% and 64% for epidermal and subepidermal layers, respectively) was observed for organically bound Cr(III) in the root tip, suggesting the occurrence of a tolerance mechanism through inclusion and chelation. The proposed models were consistent with our IP dissolution results (Fig. 6). For instance, in the root tip zone with its unique trend of organo-Cr(III) species, neither IP dissolution nor Cr release was found to occur (Figs. 4c and 6; SI-C), reinforcing the possibility of Cr re-uptake from the root tip zone in the rhizosphere. Combining the proposed models with our ICP analysis (Fig. S5b), it can be inferred that the binding of FA-like anions to Cr(III) species did not lead to increased Cr mobility and accumulation in shoot tissues.

The limited IP build-up on the root surface (Fig. 2$a_5$) is assumed to have resulted in increased binding of FA-like anions relative to Fh species to Cr ions at the adsorbing sites in the root tip epidermis (58% vs 42%; T-Spot 2 in Fig. 4c). Consequently, the formed organo-Cr(III) species transferred to the immobilising sites in the outer cell layers of the root tip (Fig. 3$a_1$). This assumption was consistent with our carbon isotope results, where the absence (or scarcity) of root plaques increased the biosynthesis and transport of $^{13}$C-labelled organic metabolites (isotopic organic carbons-Ocs) to the root system (Table 2), thereby increasing the possibility of their binding to Cr. In a study by Tao et al. (2020), it was demonstrated that a small portion of assimilated $^{13}$C was incorporated in forming organic anion metabolites involved in Cd complexation.

The reduced abundance of isotopic OCs in rice roots with IP, compared to those stored in rice roots without IP, indicated that root plaques effectively prevented the assimilation and transfer of shoot-derived metabolites (Table 2) by Cr retention and stress alleviation. Studies on plaque-free roots revealed that heavy metal stress increased the content of organic acid anions in the roots and root exudates (Yang et al., 2000; Mariano Eduardo et al., 2005).

In contrast to being a more active site of organic anion metabolism and biosynthesis (Mariano Eduardo et al., 2005), only a small fraction of total Cr in individual SOIs in the outer cell layers of the mature root could be chelated (13-17%) or exuded by these metabolites compared to iron (hydr)oxides (Fig. 4c). There was an obvious dominance of the Cr(III)-Fh complexes relative to Cr(III)-FA complexes in individual SOIs in the mature root zone, indicating the substantial role played by Fh composition of iron (hydr)oxides in conferring higher tolerance to Cr toxicity through

chelation and immobilisation (Yu et al., 2017; Zandi et al., 2020) in this region. The reduced proportion of Cr(III)-Fh complexes in the epidermal layer of the mature root, relative to the subepidermal layer of the mature root (83% vs 87%; Fig. 4c), could be explained by a higher IP dissolution and its associated Cr under the influence of the supposed metabolites in this region (Fig. 6) (Sebastian and Prasad, 2016; Saad et al., 2017).

Root surface NanoSIMS imaging demonstrated how Fe oxyhydroxide (FeO) and Cr-induced isotopic/non-isotopic OCs were closely adherent to the epidermal surface and to each other (Fig. 5). This proximity in turn indicated adsorption of organic anion metabolites or occlusion in the interstices between amorphous Fh aggregates (Zeng et al., 2008). This co-occurrence not only inhibits the growth of Fh, but also tends to form smaller amorphous aggregates, and is therefore believed to affect aggregation behaviour, surface properties and solubility/accessibility of Fh (Eusterhues et al., 2014), contributing to Fh removal and its associated Cr from the root epidermal layer (Fig. 6). Previous dissolution studies showed that organic anion metabolites adsorbed on or co-precipitated with iron (hydr)oxides were likely to weaken Cr(III)-Fe(III)-(oxy)hydroxide compositional bonds under anaerobic conditions. This phenomenon enhanced the solubility and dissolution kinetics of iron (hydr)oxides and associated dissolved Cr (Saad et al., 2017).

It is worth noting that the relationship between the secretion/exudation rate of organic anions and their root concentrations is attributed to heavy metal-activated organic anion transporter channels in the plasma membrane of root cells (Yang et al., 2012). The observed varied patterns of Cr-induced secretion of phytometabolites (Fig. 5) and IP dissolutions (Fig. 6) between the examined root regions (mature root > root tip) could be due to the fact that root exudates, regardless of their role in heavy metal chelation (Montiel-Rozas et al., 2016), are secreted to promote solubility and absorption of poorly available nutrients in the rhizosphere (Jones et al., 2004; Gojon, 2013). Indeed, the mature zone of the root system is responsible for the majority of nutrient uptake in crop plants (Jones et al., 2004; Wirth et al., 2007; Gojon, 2013), which in turn explains the absolute predominance of root exudates and dissolution rate of iron (hydr)oxides in this region compared to the root tip region (Figs. 5 and 6). In other words, the increased secretion of organic anions from the mature region compared to the immature (tip) region of the root, in addition to destabilising iron (hydr)oxides (Yang et al.,

2012, 2013) and possible release of their co-precipitated Cr ions (Fig. 6), can also be considered an essential mechanism reducing the physical resistance of root plaques to nutrient absorption.

Considering the absence of IP dissolution and release of its Cr co-precipitates (Fig. 6) and limited secretion of organic anions (Fig. 5) in the root tip region, the relatively higher proportion of organo-Cr(III) species in more internal than external tissues (64% vs 58%) of the outer cell layers in this region (Fig. 4c), likely reflected the importance of organic anions (i.e., FA-like anions) in capturing and transferring the absorbed Cr in the form of organo-Cr(III) species to the root tip sub-epidermis. The proposed model can also be construed as a possible direct or indirect re-uptake of Cr from the solution medium after release from the mature region of rice roots (as outlined earlier) and its subsequent immobilisation by a combination of Fh and FA-like chelators.

The strong presence of organo-Cr(III) (58-64%) complexes in relation to Cr(III)-Fh (36-42%) complexes in the root tip outer cell layers (Fig. 4c) was an indirect reference to the reinforcing role of FA-like anions in Cr chelation and immobilisation when the Fh chelator pool was insufficient. As indicated earlier, the accumulation of $^{13}$C-labelled organic metabolites was more intense in plaque-free roots ($^{13}$C-root) than in plaque-bearing roots (Fe$^{13}$C-root) under Cr stress, regardless of the root section (Table 2). This indirectly underscored the role played by these anions as complementary factors for Cr immobilisation.

## 5. Concluding remarks

The present study concludes that root plaques have a central role in Cr chelation and immobilisation, especially in the mature root region. The uptake inhibiting function of IP was not only confined to root epidermal surfaces but also stretched across the entire root outer cell layers. It strongly suggested that an integration of both Cr resistance (exclusion) and tolerance (chelation) strategies was directly involved in the mature region of the root, where iron (hydr)oxide precipitates alone accounted for over 83% of total Cr (Cr(III)-Fh) species at Cr hotspots in the epidermal and sub-epidermal layers of root cells. An uneven partnership in root Cr retention and inactivation was actively present in root tissues; as such, none or limited IP coated roots contained an increased amount

of isotopic OCs or a higher percentage of Cr(III)-FA species (58-64% for root tips), respectively. The proposed model concerning the outflow (Pos. mature root) or inflow (Neg. root tips) of metabolites carrying Cr (organo-Cr (III)) in outer cell layers of both root regions was well consistent (positive- Pos./ negative- Neg. effect) with signal intensities of $^{13}$C-labelled spots as active nano-scaled spots of root exudates and iron (hydr)oxide dissolution.

## Data availability

In addition to the SI, all other reasonable requests for data and research materials are available via contacting the corresponding author.

## Funding

The work was funded by the Top-Notch Young Talents Program of China, the National Natural Science Foundation of China (U1632134), the Agricultural Science and Technology Innovation Program of the Chinese Academy of Agricultural Science (2021-2025) and the National Center for Scientific Research (CNRS) in France (CNRS funded the NanoSIMS analyses). The National NanoSIMS facility at the Muséum National d'Histoire Naturelle was established by funds from CNRS, Région Ile de France, Ministère délégué à l'Enseignement Supérieur et à la Recherche, and the Muséum National d'Histoire Naturelle. Synchrotron-based microprobe analysis was conducted at the Canadian Light Source, a national research facility of the University of Saskatchewan, which is supported by the Canada Foundation for Innovation, the Natural Sciences and Engineering Research Council of Canada, the National Research Council of Canada, the Canadian Institutes of Health Research, the Province of Saskatchewan, and the University of Saskatchewan.

## CRediT authorship contribution statement

#XX and PZ equally contributed to this work.

**JY**: designed the experiments. **XX** and **PZ**: performed the lab experiments with the kind guidance of JY. **JY**, **XX** and **PZ**: performed the XRF, XANES and SEM measurements and data

analysis. **JY**, **JL**, **RL** and **CR**: conducted the NanoSIMS experiments. **JY**, **JL** and **XX**: performed the NanoSIMS data analysis. **PZ**, XX, **JY** and **JL**: analysed the data and drafted the manuscript. **JY**, **PZ**, **BE**, **ES** and **BBK**: participated in the interpretation of results. **JY**, **CR**, **RL**, **PZ**, **BE**, **ES** and BBK: improved the grammar and corrected spelling mistakes. **PZ**, **JY**, XX, **BE**, **BBK** and **ES**: edited and thoroughly revised the manuscripts. All authors read, corrected and approved the final submitted version of the manuscript.

## Declaration of Competing Interest

The authors declare that they have no known competing financial interests or personal relationships that could have appeared to influence the work reported in this paper.

## References


Agnello, A., Huguenot, D., Van Hullebusch, E., Esposito, G., 2014. Enhanced phytoremediation: a review of low molecular weight organic acids and surfactants used as amendments. Crit. Rev. Environ. Sci. Technol. 44, 2531e2576. https://dx.doi.org/10.1080/10643389.2013.829764.

Ali, W., Zhang, H., Mao, K., Shafeeque, M., Aslam, M.W., Yang, X., Zhong, L., Feng, X., Podgorski, J., 2022. Chromium contamination in paddy soil-rice systems and associated human health risks in Pakistan. Sci. Total Environ. 826,153910. https://doi.org/10.1016/j.scitotenv.2022.153910.

Amaral, D.C., Lopes, G., Guilherme, L.R.G., Seyfferth, A.L., 2017. A new approach to sampling intact Fe plaque reveals Si-induced changes in Fe mineral composition and shoot as in rice. Environ. Sci. Technol. 51, 38–45. https://doi.org/10.1021/acs.est.6b03558

Assimakopoulou, A., Kotsiras, A., Nifakos, K., 2013. Incidence of lettuce tipburn as related to hydroponic system and cultivar. J. Plant Nutr. 36(9), 1383–1400. https://doi.org/10.1080/01904167.2013.793709

Bali, A.S., Sidhu, G.P.S., Kumar, V., 2020. Root exudates ameliorate cadmium tolerance in plants: A review. Environ. Chem. Lett. 18, 1243–1275. https://doi.org/10.1007/s10311-020-01012-x

Banakar, R., Fernandez, A.A., Díaz-Benito, P., Abadia, J., Capell, T., Christou, P., 2017.

659 Phytosiderophores determine thresholds for iron and zinc accumulation in biofortified rice
660 endosperm while inhibiting the accumulation of cadmium. J. Exp. Bot. 68(17), 4983–
661 4995. https://doi.org/10.1093/jxb/erx304
662 Becker, M., Ngo, N.S., Schenk, M.K.A., 2020. Silicon reduces the iron uptake in rice and induces
663 iron homeostasis related genes. Sci. Rep. 10, 5079. https://doi.org/10.1038/s41598-020-61718-4
664 Briat, J.F., Ravet, K., Arnaud, N., Duc, C., Boucherez, J., Touraine, B., Cellier, F., Gaymard, F., 2010.
665 New insights into ferritin synthesis and function highlight a link between iron homeostasis and
666 oxidative stress in plants. Ann. Bot. 105, 811–822. https://doi.org/10.1093/aob/mcp128
667 Cao, Z.Z., Qin, M.L., Lin, X.Y., Zhu, Z.W., Chen, M.X., 2018. Sulfur supply reduces cadmium
668 uptake and translocation in rice grains (*Oryza sativa* L.) by enhancing iron plaque formation,
669 cadmium chelation vacuolar sequestration. Environ. Pollut. 238, 76–84.
670 https://doi.org/10.1016/j.envpol.2018.02.083
671 Chen, K., Li, B., He, G., 2000. High-yielding cultivation techniques for a new high-quality rice
672 variety Xiangzaoxian No. 31. Crop Res. 4, 43. https://doi.org/10.16848/j.cnki.issn.1001-
673 5280.2000.04.017. [in Chinese]
674 Chen, Y.T., Wang, Y., Yeh, K.C., 2017. Role of root exudates in metal acquisition and tolerance.
675 Curr. Opin. Plant Biol. 39, 66–72. https://doi.org/10.1016/j.pbi.2017.06.004
676 Cheng, H., Wang, M., Wong, M.H., Ye, Z., 2014. Do radial oxygen loss and iron plaque formation
677 on roots alter Cd and Pb uptake and distribution in rice plant tissues? Plant Soil 375, 137–148.
678 https://doi.org/10.1007/s11104-013-1945-0
679 Coudert, Y., Périn, C., Courtois, B., Khong, N.G., Gantet, P., 2010. Genetic control of root
680 development in rice, the model cereal. Trend Plant Sci. 15(4), 219–226. https://doi.org/
681 10.1016/j.tplants.2010.01.008.
682 Crowder, A.A., Coltman, D.W., 1993. Formation of manganese oxide plaque on rice roots in solution
683 culture under varying pH and manganese ($Mn^{2+}$) concentration conditions. J. Plant Nutr. 16 (4),
684 589–599. https://doi.org/10.1080/01904169309364559
685 Deng, D., Wu, S.C., Wu, F.Y., Deng, H., Wong, M.H., 2010. Effects of root anatomy and Fe plaque
686 on arsenic uptake by rice seedlings grown in solution culture. Environ. Pollut. 158, 2589–2595.

https://doi.org/10.1016/j.envpol.2010.05.015.

Eusterhues, K., Hädrich, A., Neidhardt, J., Küsel, K., Keller, T.F., Jandt, K.D., Totsche, K.U., 2014. Reduction of ferrihydrite with adsorbed and coprecipitated organic matter: microbial reduction by Geobacter bremensisvs. Abiotic reduction by Na-dithionite. Biogeosciences 11, 4953–4966. https://doi.org/10.5194/bg-11-4953-2014

Frommer, J., Voegelin, A., Dittmar, J., Marcus, M.A., Kretzschmar, R., 2011. Biogeochemical processes and arsenic enrichment around rice roots in paddy soil: results from micro-focused X-ray spectroscopy. Eur. J. Soil Sci. 62, 305–317. https://doi.org/10.1111/j.1365-2389.2010.01328.x

Fukao, T., Barrera-Figueroa, B.E., Juntawong, P., Peña-Castro, J.M., 2019. Submergence and waterlogging stress in plants: a review highlighting research opportunities and understudied aspects. Front. Plant Sci. 10, 340. https://doi.org/10.3389/fpls.2019.00340

Ge, T., Yuan, H., Zhu, H., Wu, X., Nie, S., Liu, C., Tong, C., Wu, J., Brookes, P., 2012. Biological carbon assimilation and dynamics in a flooded rice–soil system. Soil Biol. Biochem. 48, 39–46. https://doi.org/10.1016/j.soilbio.2012.01.009

Geng, Z., Wang, P., Fu, Y.,Liu, W., Cui, Y., 2020. Bioaccessibility of chromium in rice and Its human health risk assessment, Asian J. Ecotoxicol. (6), 205–211. https://doi.org/10.7524/AJE.1673-5897.20190610002

Gojon, A., 2013. Inorganic Nitrogen acquisition and signalling. In: Eshel, A., Beeckman, T. (Eds.), Plant Roots. CRC Press, Boca Rotan, pp. 1–14.

Gu, D., Zhen, F., Hannaway, D.B., Zhu, Y., Liu, L., Cao, W., Tang, L., 2017. Quantitative classification of rice (*Oryza sativa* l.) root length and diameter using image analysis. PLoS One 12(1), e0169968. https://doi.org/10.1371/journal.pone.0169968.

Gunnars, A., Blomqvist, S., Johansson, P., Andersson, C., 2002. Formation of Fe (III) oxyhydroxide colloids in fresh water and brackish seawater, with incorporation of phosphate and calcium. Geochim. Cosmochim. Acta 66, 745–758. https://doi.org/10.1016/S0016-7037(01)00818-3

713 Hayat, S., Khalique, G., Irfan, M., Wani, A.S., Tripathi, B.N., Ahmad, A., 2012. Physiological
714 changes induced by chromium stress in plants: an overview. Protoplasma 249, 599–611.
715 https://doi.org/10.1007/s00709-011-0331-0
716 Hepler, P.K., 2005. Calcium: A central regulator of plant growth and development. Plant Cell. 17(8),
717 2142–2155. https://doi.org/10.1105/tpc.105.032508
718 Holland, S.L., Avery, S.V., 2011. Chromate toxicity and the role of sulfur. Metallomics 3, 1119–1123.
719 https://doi.org/10.1039/c1mt00059d
720 Holzschuh, M.J., Carlos, F.S., Carmona, F.C., Bohnen, H., Anghinoni, I., 2014. Iron oxidation on the
721 surface of adventitious roots and its relation to aerenchyma formation in rice genotypes. Revista
722 Brasileira de Ciência do Solo 38 (1), 185–192. https://doi.org/10.1590/S0100-
723 06832014000100018
724 Hu, Y., Huang, Y.Z., Liu Y.X., 2014. Influence of iron plaque on chromium accumulation and
725 translocation in three rice (*Oryza sativa* L.) cultivars grown in solution culture. Chem. Ecol. 30
726 (1), 29–38. https://doi.org/10.1080/02757540.2013.829050
727 Jones, D.L., Hodge, A., Kuzyakov, Y., 2004. Plant and mycorrhizal regulation of
728 rhizodeposition. New Phytol. 163 (3), 459–480. https://doi.org/10.1111/j.1469-
729 8137.2004.01130.x
730 Kaiser, C., Kilburn, M.R., Clode, P.L., Fuchslueger, L., Koranda, M., Cliff, J.B., Solaiman, Z.M.,
731 Murphy, D.V., 2015. Exploring the transfer of recent plant photosynthates to soil microbes:
732 mycorrhizal pathway vs. direct root exudation. New Phytol. 205, 1537–1551.
733 https://doi.org/10.1111/nph.13138
734 Khan, F.H., Ambreen, K., Fatima, G. and Kumar, S., 2012. Assessment of health risks with reference
735 to oxidative stress and DNA damage in chromium exposed population. Sci. Total Environ. 430,
736 68–74. https://doi.org/10.1016/j.scitotenv.2012.04.063
737 Khan, N., Seshadri, B., Bolan, N., Saint, C.P., Kirkham, N.B., Chowdhury, S., Yamaguchi, N., Lee,
738 D.Y., Li, G., Kunhikrishnan, A., Qi, F., Karunanithi, R., Qiu, R., Zhu, Y.G., Syu, C.H., 2016.
739 Root iron plaque on wetland plants as a dynamic pool of nutrients and contaminants. Adv. Agron.

138, 1–96. https://doi.org/10.1016/bs.agron.2016.04.002

Li, J., Jia, Y., Dong, R., Huang, R., Liu, P., Li, X., Wang, Z., Liu, G., Chen. Z., 2019. Advances in the mechanisms of plant tolerance to manganese toxicity. Int. J. Mol. Sci. 20(20), 5096. https://doi.org/10.3390/ijms20205096

Li., Y., Zhao, J., Zjang, B., Liu, Y., Xu, X., Li, Y.F., Li, B., Gao, Y., Chai, Z., 2015. The influence of iron plaque on the absorption, translocation and transformation of mercury in rice (*Oryza sativa* L.) seedlings exposed to different mercury species. Plant Soil 398, 87–97. https://doi.org/10.1007/s11104-015-2627-x

Liu, W.J., Zhu, Y.G., 2005. Iron and Mn plaques on the surface of roots of wetland plants. Acta Ecol. Sin. 25 (2), 358–363. (In Chinese)

Liu, W.J., Zhu, Y.G., Smith, F.A., Smith, S.E., 2004. Do phosphorus nutrition and iron plaque alter arsenate (As) uptake by rice seedlings in hydroponic culture? New Phytol. 162, 481–488. https://doi.org/10.1111/j.1469-8137.2004.01035.x

Lombi, E., Susini, J., 2009. Synchrotron-based techniques for plant and soil science: opportunities, challenges and future perspectives. Plant Soil 320, 1–35. https://doi.org/10.1007/s11104-008-9876-x

Lu, L., Xie, R., Liu, T., Wang, H., Hou, D., Du, Y., He, Z., Yang, X., Sun, H., Tian, S., 2017. Spatial imaging and speciation of Cu in rice (*Oryza sativa* L.) roots using synchrotron-based X-ray microfluorescence and X-ray absorption spectroscopy. Chemosphere 175, 356–364. https://doi.org/10.1016/j.chemosphere.2017.02.082.

Luo, Q., Wang, S., Sun, L., Wang, H., 2017. Metabolic profiling of root exudates from two ecotypes of *Sedum alfredii* treated with Pb based on GC-MS. Sci. Rep. 7, 39878. https://doi.org/10.1038/srep39878

Mariano Eduardo, D., Jorge Renato, A., Keltjens Willem, G., Marcelo, M., 2005. Metabolism and root exudation of organic acid anions under aluminium stress. Braz. J. Plant Physiol. 17, 157–172. https://doi.org/10.1590/S1677-04202005000100013.

Montiel-Rozas, M.M., Madejón, E., Madejón, P., 2016. Effect of heavy metals and organic matter on root exudates of herbaceous species: An assessment in sand and soil conditions under different

levels of contamination. Environ. Pollut. 216, 273–281. https://doi.org/10.1016/j.envpol.2016.05.080

Nickens, K.P., Patierno, S.R. and Ceryak, S., 2010. Chromium genotoxicity: a double-edged sword. Chem. Biol. Interact., 188(2), 276–288. https://doi.org/10.1016/j.cbi.2010.04.018

Nishiuchi, S., Yamauchi, T., Takahashi, H., Kotula, L., Nakazono, M., 2012. Mechanisms for coping with submergence and waterlogging in rice. Rice 5, 2. https://doi.org/10.1186/1939-8433-5-2

Osmolovskaya, N., Dung, V.V., Kuchaeva, L., 2018. The role of organic acids in heavy metal tolerance in plants. Bio. Comm. 63 (1), 9–16. https://doi.org/10.21638/spbu03.2018.103

Pathak, R.K., Singh, D.B., Sharma, H., Pandey, D., Dwivedi, S., 2021. Calcium uptake and translocation in plants. In: Upadhyay, S.K. (Ed.), Calcium Transport Elements in Plants, 1st, ed. Academic Press, New York, pp. 373–386.

Peng, C., Duan, D., Xu, C., Chen, Y., Sun, L., Zhang, H., Yuan, X., Zheng, L., Yang, Y., Yang, J., Zhen, X., Chen, Y., Shi, J., 2015. Translocation and biotransformation of CuO nanoparticles in rice (*Oryza sativa* L.) plants. Environ. Pollut. 197, 99–107. https://doi.org/10.1016/j.envpol.2014.12.008.

Pradas del Real, A.E., García-Gonzalo, P., Lobo, M.C., Pérez-Sanz, A., 2014. Chromium speciation modifies root exudation in two genotypes of *Silene vulgaris*. Environ. Exp. Bot. 107, 1−6. https://doi.org/10.1016/j.envexpbot.2014.05.002

Qin, Y., Zhu, H., Zhang, M., Zhang, H., Xiang, C., Li, B., 2016. GC-MS analysis of membrane-graded fulvic acid and Its activity on promoting wheat seed germination. Molecules 21(10), 1363. https://doi.org/10.3390/molecules21101363

Rashid, I., Murtaza, G., Zahir, Z.A., Farooq, M., 2018. Effect of humic and fulvic acid transformation on cadmium availability to wheat cultivars in sewage sludge amended soil. Environ. Sci. Pollut. Res. 25, 16071–16079. https://doi.org/10.1007/s11356-018-1821-9.

Ravel, B., Newville, M., 2005. Athena, Artemis, Hephaestus: data analysis for X-ray absorption spectroscopy using IFEFFIT. J. Synchrotron Rad. 12, 537–541. https://doi.org/10.1107/S0909049505012719

Saad, E.M., Sun, J., Chen, S., Borkiewicz, O.J., Zhu, M., Duckworth, O.W., Tang, Y., 2017. Siderophore and organic acid promoted dissolution and transformation of Cr(III)-Fe (III)-(oxy) hydroxides. Environ. Sci. Technol. 51 (6), 3223–3232. https://doi.org/10.1021/acs.est.6b05408

Seal, A.N., Haig, T., Pratley, J.E., 2004. Evaluation of putative allelochemicals in rice root exudates for their role in the suppression of Arrowhead root growth. J. Chem. Ecol. 30, 1663–1678. https://doi.org/10.1023/B:JOEC.0000042075.96379.71

Sebastian, A., Prasad, M.N.V., 2016. Iron plaque decreases cadmium accumulation in *Oryza sativa* L. and serves as a source of iron. Plant Biol. 18 (6), 1008–1015. https://doi.org/10.1111/plb.12484.

Seyfferth, A.L., Webb, S.M., Andrews, J.C., Fendorf, S., 2010. Arsenic localization, speciation, and co-occurrence with iron on rice (*Oryza sativa* l.) roots having variable Fe coatings. Environ. Sci. Technol. 44, 8108–8113. https://doi.org/10.1021/es101139z

Somenahally, A.C., Hollister, E.B., Yan, W., Gentry, T.J., Loeppert, R.H., 2011. Water management impacts on arsenic speciation and iron-reducing bacteria in contrasting rice-rhizosphere compartments. Environ. Sci. Technol. 45, 8328–8335. https://doi.org/10.1021/es2012403

Tang, Y.Z., Michel, F.M., Zhang, L.H., Harrington, R., Parise, J.B., Reeder, R.J., 2010. Structural properties of the Cr(III)-Fe(III) (oxy)hydroxide compositional series: Insights for a Nanomaterial "solid solution". Chem. Mat. 22 (12), 3589–3598. https://doi.org/10.1021/cm1000472

Tao, Q., Zhao, J., Jinxing, L., Liu, Y., Luo, J., Yuan, S., Li, B., Li, Q., Xu, Q., Yu, X., Huang, H., Li, T., 2020. Unique root exudate tartaric acid enhanced cadmium mobilization and uptake in Cd-hyperaccumulator *Sedum alfredii*. 383, 121177. https://doi.org/10.1016/j.jhazmat.2019.121177

Tian, S., Lu, L., Yang, X., Webb, S.M., Du, Y., Brown, P.H., 2010. Spatial imaging and speciation of lead in the accumulator plant *Sedum alfredii* by microscopically focused synchrotron X-ray investigation. Environ. Sci. Technol. 44(15), 5920–5926. https://doi.org/10.1021/es903921t

Tripathi, R.D., Tripathi, P., Dwivedi, S., Kumar, A., Mishra, A., Chauhan, P.S., Norton, G.J., Nautiyal, C.S., 2014. Roles for root iron plaque in sequestration and uptake of heavy metals and metalloids in aquatic and wetland plants. Metallomics 6, 1789–1800. https://doi.org/10.1039/c4mt00111g

Uren, N.C., 2000. Types, amount, and possible functions of compounds released into the rhizosphere by soil-grown plants. In: Pinton, R., Varanini, Z., Nannipieri, P. (Eds.), The Rhizosphere: Biochemistry and Organic Substances at the Soil–Plant Interface. Marcel Dekker, New York, pp. 19–40.

van Genuchten, C.M., Gadgil, A.J., Peña, J., 2014. Fe (III) nucleation in the presence of bivalent 12 cations and oxyanions leads to subnanoscale 7 Å polymers. Environ. Sci. Technol. 48, 11828–11836. https://doi.org/10.1021/es503281a

Wang, Y., Yang, J., Han, H., Hu, Y., Wang, J., Feng, Y., Yua, B., Xia, X., Darma, A., 2021. Differential transformation mechanisms of exotic Cr(VI) in agricultural soils with contrasting physio-chemical and biological properties. Chemosphere 729, 130546 https://doi.org/10.1016/j.chemosphere.2021.130546

Wang, Y., Yang, R., Zheng, J., Shen, Z., Xu, X., 2019. Exogenous foliar application of fulvic acid alleviate cadmium toxicity in lettuce (*Lactuca sativa* L.). Ecotoxicol. Environ Saf. 167,10–19. https://doi.org/10.1016/j.ecoenv.2018.08.064.

Williams, P.N., Santner, J., Larsen, M., Lehto, N.J., Oburger, E., Wenzel, W., Glud, R.N., Davison, W., Zhang, H., 2014. Localised flux maxima of arsenic, lead, and iron around root apices in flooded lowland rice. Environ. Sci. Technol. 48 (15), 8498–8506. https://doi.org/10.1021/es501127k

Wirth, J., Chopin, F., Santoni, V., Viennois, G., Tillard, P., Krapp, A., Lejay, L., Daniel-Vedele, F., Gojon, A., 2007. Regulation of root nitrate uptake at the NRT2.1 protein level in *Arabidopsis thaliana*. J. Biol. Chem. 282, 23541–23552. https://doi.org/10.1074/jbc.M700901200

Wu, C., Ye, Z., Li, H., Wu, S., Deng, D., Zhu, Y., Wong, M., 2012. Do radial oxygen loss and external aeration affect iron plaque formation and arsenic accumulation and speciation in rice? J. Exp. Bot. 63, 2961–2970. https://doi.org/10.1093/jxb/ers017.

Xiao, W., Ye, X., Zhu, Z., Zhang, Q., Zhao, S., Chen, D., Gao, N., Hu, J., 2021. Continuous flooding stimulates root iron plaque formation and reduces chromium accumulation in rice (*Oryza sativa* L.). Sci. Total Environ. 788,147786. https://doi.org/10.1016/j.scitotenv.2021.147786

Xiao, W., Zhang, Q., Zhao, S., Chen, D., Gao, N., Huang, M., Ye, X., 2023. Citric acid secretion from rice roots contributes to reduction and immobilization of Cr(VI) by driving microbial sulfur and iron cycle in paddy soil. Sci. Total Environ.16,158832. https://doi.org/10.1016/j.scitotenv.2022.158832.

Xu, B., Wang, F., Zhang, Q., Lan, Q., Liu, C., Guo, X., Cai, Q., Chen, Y., Wang, G., Ding, J., 2018. Influence of iron plaque on the uptake and accumulation of chromium by rice (*Oryza sativa* L.) seedlings: Insights from hydroponic and soil cultivation. Ecotoxicol Environ. Saf. 162, 51–58. https://doi.org/10.1016/j.ecoenv.2018.06.063

Xu, B., Yu, S., 2013. Root iron plaque formation and characteristics under N2 flushing and its effects on translocation of Zn and Cd in paddy rice seedlings (*Oryza sativa*). Ann. Bot., 111(6):1189–1195. doi:10.1093/aob/mct072

Xu, M., Gao, P., Wu, J., Ma, J., Zhang, X., Yang, G., Long, L., Chen, C., Song, C., Xiao, Y., 2022. Biochar promotes arsenic sequestration on iron plaques and cell walls in rice roots. Chemosphere 288, 132422. https://doi.org/10.1016/j.chemosphere.2021.132422

Yamaji, N., Ma, J.F., 2007. Spatial distribution and temporal variation of the rice silicon transporter Lsi1. Plant Physiol. 143, 1306–1313. https://doi.org/10.1104/pp.106.093005

Yang, J., Xia, X., Liu, J., Wang, J., Hu, Y., 2020. Molecular mechanisms of chromium (III) immobilization by organo–ferrihydrite co-precipitates: The significant roles of ferrihydrite and carboxyl. Environ. Sci. Technol. 54 (8), 4820–4828. https://doi.org/10.1021/acs.est.9b06510

Yang, J., Zhu, S., Zheng, C., Sun, L., Liu, J., Shi, J., 2015. Impact of S fertilizers on pore-water Cu dynamics and transformation in a contaminated paddy soil with various flooding periods. J. Hazard. Mater. 286, 432–439. https://doi.org/10.1016/j.jhazmat.2015.01.035

Yang, L.T., Jiang, H.X., Qi, Y.P., Chen, L.S., 2012. Differential expression of genes involved in alternative glycolytic pathways, phosphorus scavenging and recycling in response to aluminium and phosphorus interactions in citrus roots. Mol. Biol. Rep. 39 (5), 6353–6366. https://doi.org/10.1007/s11033-012-1457-7.

Yang, L.T., Qi, Y.P., Jiang, H.X., Chen, L.S., 2013. Roles of organic acid anion secretion in

aluminium tolerance of higher plants. Biomed. Res. Int. 2013, 173682. https://doi.org/10.1155/2013/173682

Yang, S., Zhao, J., Chang, S.X., Collins, C., Xu, J., Liu, X., 2019a. Status assessment and probabilistic health risk modeling of metals accumulation in agriculture soils across China: A synthesis. Environ. Int. 128, 165–174. https://doi.org/10.1016/j.envint.2019.04.044

Yang, Y., Yang, Z., Yu, S., Chen, H., 2019b. Organic acids exuded from roots increase the available potassium content in the rhizosphere soil: a rhizobag experiment in *Nicotiana tabacum*. *Hort. Sci.* *54*, 23–27. https://doi.org/10.21273/HORTSCI13569-18

Yang, Y.Y., Jung, J.Y., Song, W.Y., Suh, H.S., Lee, Y., 2000. Identification of rice varieties with high tolerance or sensitivity to lead and characterization of the mechanism of tolerance. Plant Physiol. 124, 1019–1026. https://doi.org/10.1104/pp.124.3.1019

Ye, Z.H., Cheung, K.C., Wong, M.H., 2001. Copper uptake in *Typha latifolia* as affected by iron and manganese plaque on the root surface. Can. J. Bot. 79, 314–320. https://doi.org/10.1139/b01-012

Yu, X.Z., Lu, M.R., Zhang, X.H., 2017. The role of iron plaque in transport and distribution of chromium by rice seedlings. Cereal Res. Commun. 45 (4), 598–609. https://doi.org/10.1556/0806.45.2017.040

Yu, Y., 2018. History of Chinese Rice Varieties (Hunan Conventional Rice Rolls), first ed. China Agriculture Press, China.

Yuan, H., Zhu, Z., Liu, S., Ge, T., Jing, H., Li, B., Liu, Q., Lynn, T.M., Wu, J., Kuzyakov, Y., 2016. Microbial utilization of rice root exudates: 13C labeling and PLFA composition. Biol. Fertil. Soils 52, 615–627. https://doi.org/10.1007/s00374-016-1101-0

Zandi, P., Yang, J., Darma, A., Bloem, E., Xia, X., Wang, Y., Li, Q., Schnug, E., 2022. Iron plaque formation, characteristics, and its role as a barrier and/or facilitator to heavy metal uptake in hydrophyte rice (*Oryza sativa* L.). Environ. Geochem. Health. https://doi.org/10.1007/s10653-022-01246-4.

Zandi, P., Yang, J., Xia, X., Barabasz-Krasny, B., Możdżeń, K., PuŁa, J., Elke, B., Wang, Y., Hussain, S., Hashemi, S.M., Różanowski, B., Qian, L., 2021. Sulphur nutrition and iron plaque formation on roots of rice seedlings and their consequences for immobilisation and uptake of

chromium in solution culture. Plant Soil 462, 365–388. https://doi.org/10.1007/s11104-021-04870-8

Zandi, P., Yang, J.J., Xin, X., Yu, T., Li, Q., Możdżeń, K., Barabasz-Krasny, B., Yaosheng, W., 2020. Do sulfur addition and rhizoplane iron plaque affect chromium uptake by rice (*Oryza sativa* L.) seedlings in culture solution? J. Hazard. Mater. 2020, 121803. https://doi.org/10.1016/j.jhazmat.2019.121803

Zeng, F., Chen, S., Miao, Y., Wu, F., Zhang, G., 2008. Changes of organic acid exudation and rhizosphere pH in rice plants under chromium stress. Environ. Pollut. 155 (2), 284–289. https://doi.org/10.1016/j.envpol.2007.11.019

Zeng, F., Zhou, W., Qiu, B., Ali, S.,Wu, F., Zhang, G., 2011. Subcellular distribution and chemical forms of chromium in rice plants suffering from different levels of chromium toxicity. J. Plant Nutr. Soil Sci. 174, 249–256. https://doi.org/10.1002/jpln.200900309

Zhang, Q., Liu, J., Lu, H., Zhao, S., Wang, W., Du, J., Yan, C., 2015. Effects of silicon on growth, root anatomy, radial oxygen loss (ROL) and Fe/Mn plaque of *Aegiceras corniculatum* (L.) Blanco seedlings exposed to cadmium. Environ. Nanotechnol. Monitor. Manag. 4, 6–11. https://doi.org/10.1016/j.enmm.2015.04.001

Zhang, Z., Shi, W., Ma, H., Zhou, B., Li, H., Lü, C., He, J., 2020. Binding mechanism between fulvic acid and heavy metals: integrated interpretation of binding experiments, fraction characterizations, and models. Water Air Soil Pollut. 231,184. https://doi.org/10.1007/s11270-020-04558-2

Zhao, F., Ma, Y., Zhu, Y.G., Tang, Z., Mcgrath, S.P., 2015. Soil contamination in China, current status and mitigation strategies. Environ. Sci. Technol. 49 (2), 750–759. https://doi.org/10.1021/es5047099

## Table Captions

**Table 1** Cr and Fe concentrations and percentage distributions in different organs of the rice plant

**Table 2** $\delta^{13}C$ values (‰), percentage of non-isotopic carbon and $^{13}C$ abundance for labelled/unlabelled rice shoot and root (with or without iron plaque) samples

**Table 1**

| Treatments | DCB extracts (iron plaque) | | | | Roots | | | | Shoots | | | |
|---|---|---|---|---|---|---|---|---|---|---|---|---|
| | Concentration (mg $kg^{-1}$) | | Distribution (%) | | Concentration (mg $kg^{-1}$) | | Distribution (%) | | Concentration (mg $kg^{-1}$) | | Distribution (%) | |
| | Cr | Fe | Cr | Fe | Cr | Fe | Cr | Fe | Cr | Fe | Cr | Fe |
| Fe80-CK | 0.00b ±0.00 | 41.26b ± 2.80 | – | 90.7 | 0.00b ± 0.00 | 1.95ab ±0.43 | – | 4.3 | 0.00b ± 0.00 | 0.40a ± 0.04 | – | 5.0 |
| Fe80-Cr(III) | 1.89a ±0.14 | 62.73a ±2.60 | 37.3 | 88.7 | 2.66a ± 0.14 | 3.87a ±0.65 | 53.0 | 5.3 | 0.04a ± 0.00 | 0.34a ± 0.01 | 9.7 | 6.0 |
| LSD % | 0.60 | 20.74 | 9.41 | 8.72 | 0.61 | 4.66 | 16.16 | 4.30 | 0.01 | 0.21 | 7.59 | 5.17 |

*Notes*. Data are means ± SE (n=3); DCB, dithionite–citrate–bicarbonate, CK and Cr (III) represent 0 and 1.0 mg $L^{-1}$ $CrCl_3$. $6H_2O$, respectively; Fe80 represents 80 mg $L^{-1}$ $FeSO_4 \cdot 7H_2O$; data are means of 3 replications; different small letters indicate a significant difference at $p$ <0.05 according to the LSD test.

**Table 2**

| Plant Sample (PS) | $^{*}\delta^{13}C$ (‰) | $^{**}C\%$ (μg C $g^{-1}$ of a PS)×100 | $^{13}C$ abundance (μg $^{13}C$ $g^{-1}$ PS C) |
|---|---|---|---|
| CK-root | –30 | 46.09 | 1.08 |
| $^{13}C$-root | 515 | 45.54 | 1.67 |
| $Fe^{13}C$-root | 456 | 23.25 | 1.61 |
| CK-shoot | –32.99 | 43.05 | 1.08 |
| $^{13}C$-shoot | 1968 | 44.47 | 3.23 |

*Note.* $^{*}$- [(molar ratio of $^{13}C/^{12}C$ in samples divided by the carbonate-based VPDB standards) –1×1000]; CK-unlabelled ($^{12}C$) plant samples; $^{**}$- denotes the mass content percentage of C in plant samples.

# Figure captions

**Fig. 1.** The concentrations of Fe (a) and Cr (b) in root tip and mature root regions before (in iron plaque) and after (in root tissues) DCB extraction in *Oryza. sativa* L. at the seedling stage. Bars labelled with different lowercase letters are considered significant at $p < 0.05$. Data points and bars represent means ± SE (n=3).

**Fig. 2.** (a)-Microscale distribution (μ-XRF mapping) of Cr ($a_{1,4}$), Fe ($a_{2,5}$), and Ca ($a_{3,6}$) on the epidermal surface of mature and tip regions of rice roots with iron plaque, and under Cr(III) treatment. (b)-Correlation between the intensities of Cr with Fe ($b_{1,4}$) and Ca ($b_{2,5}$) as well as Fe with Ca ($b_{3,6}$) within maps of the root tip and mature sections quantified by μ-XRF analysis. Scale bars ranging from dark blue (low counts) to dark red (high counts) colours for each element were acquired from fluorescence intensities. Each image reports the relative distribution map of individual elements.

**Fig. 3.** Two-dimensional μ-XRF elemental distribution maps for cross-sections of the root tip and mature root regions in rice seedlings after Fe80-Cr(III) treatment. Hot spot regions are marked by red "X" and labelled in both the root tip (1, 2) and mature (1, 2) root cross-sections. Red boxes in the upper images show where μ-XRF maps were obtained. The selected regions with relatively higher concentrations of Cr are referred to those of positions subjected to μ-X-ray absorption near-edge spectroscopy (μ-XANES) spectra collection. Scale bars representing different colours (dark blue-low counts to dark red-high counts) for each element were acquired from fluorescence intensities. Each image reports the relative distribution map of individual elements.

**Fig. 4.** Chromium (Cr) K-edge XANES spectra (a) and their first derivative spectra (b) from Cr hotspots (in Fig. 3$a_{1\text{-}2}$) in the root tip (T) and mature (M) root cross-sections, as well as the Cr reference standards (Cr(III) bound to ferrihydrite (Fh) or fulvic acid (FA, referred to as organo-Cr(III) complexes) and a Cr(III) compound ($Cr(CH_3COO)_3$). The linear combination fitting (LCF) results are

shown in (c). The experimental and fitting XANES spectra in the subgraph (c) are shown as solid and dashed lines, respectively. R factor represents a goodness-of-fit parameter.

**Fig. 5.** Elemental maps of $^{12}C^{14}N$, $^{13}C^{14}N$, $^{52}Cr^{16}O$, and $^{56}Fe^{16}O$ and corresponding RGB maps, measured by NanoSIMS, illustrating the overlapping of Cr, Fe and $^{13}C$ hotspots (C-green, Cr -red, Fe-blue) in cross-sections of mature root (white dotted circles in image a) and root tip (white arrows in image b) regions in rice seedlings after Fe80-Cr(III) treatment. $^{13}C$-labelled spots in bioimaging of root cross-sections reflect the active nano-scaled spot of root exudates (phyto-metabolites) secreting from root epidermis.

**Fig. 6.** The concentration ratio of Fe/Cr to the calcium (Ca) in the iron plaque of different root sections during several days after Fe80-Cr (III) treatment. Markers labelled with different lowercase letters are considered significant at $p < 0.05$. Error bars represent ± SD (n=2). (Fe/Ca and Cr/Ca ratios were calculated to minimise the impact of varied root weights on the determined Fe and Cr concentrations at the corresponding harvesting time).

**Figure 1**

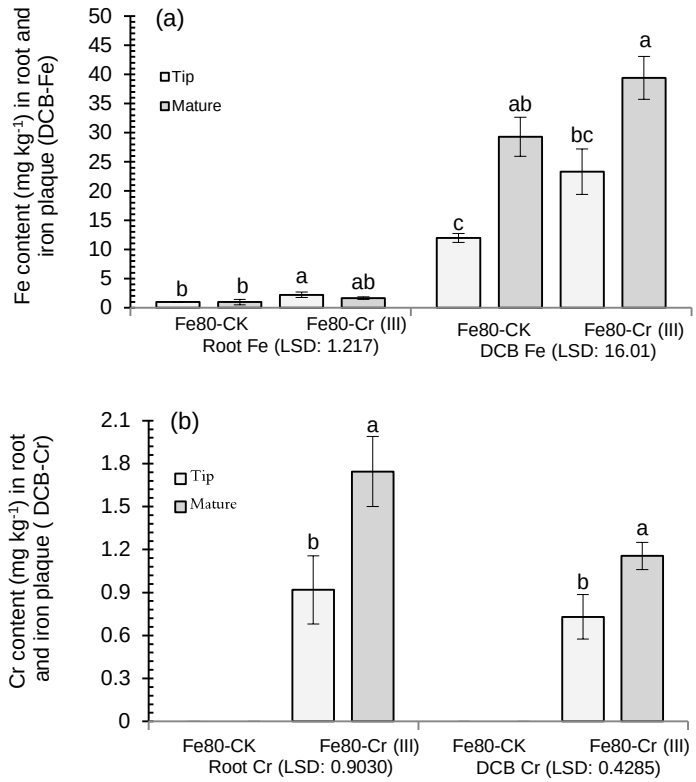
(a)
Tip
Mature
Fe content (mg kg-1) in root and iron plaque (DCB-Fe)
50
45
40
35
30
25
20
15
10
5
0
b
b
a
ab
c
ab
bc
a
Fe80-CK
Fe80-Cr (III)
Root Fe (LSD: 1.217)
Fe80-CK
Fe80-Cr (III)
DCB Fe (LSD: 16.01)
(b)
Tip
Mature
Cr content (mg kg-1) in root and iron plaque ( DCB-Cr)
2.1
1.8
1.5
1.2
0.9
0.6
0.3
0
b
a
b
a
Fe80-CK
Fe80-Cr (III)
Root Cr (LSD: 0.9030)
Fe80-CK
Fe80-Cr (III)
DCB Cr (LSD: 0.4285)

## Figure 2

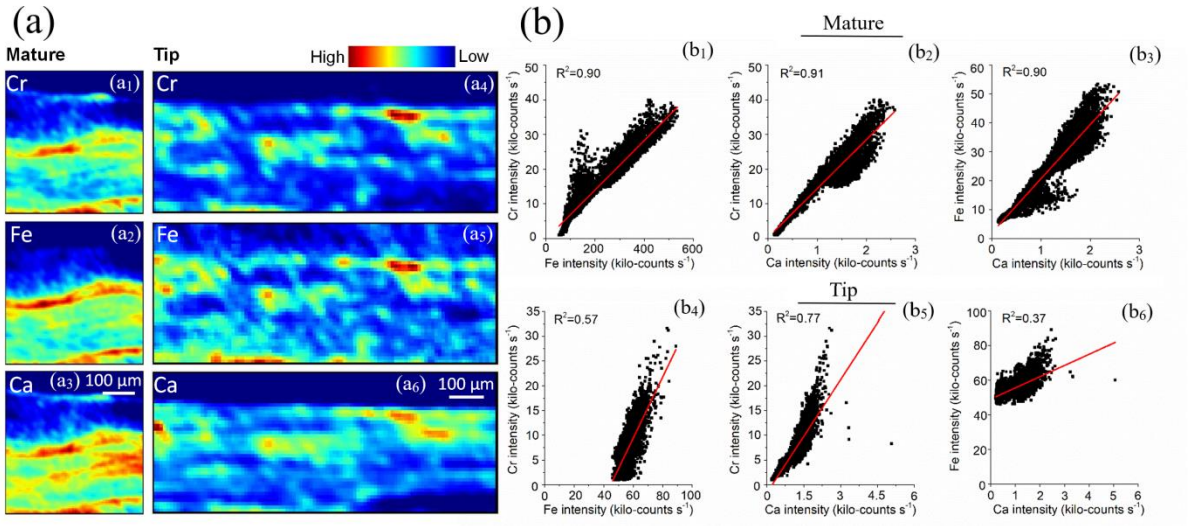
(a)
Mature
Tip
High
Low
Cr
(a1)
Fe
(a2)
Ca
(a3) 100 µm
Cr
(a4)
Fe
(a5)
Ca
(a6) 100 µm
(b)
Mature
(b1)
R2=0.90
Cr intensity (kilo-counts s-1)
Fe intensity (kilo-counts s-1)
(b2)
R2=0.91
Cr intensity (kilo-counts s-1)
Ca intensity (kilo-counts s-1)
(b3)
R2=0.90
Fe intensity (kilo-counts s-1)
Ca intensity (kilo-counts s-1)
Tip
(b4)
R2=0.57
Cr intensity (kilo-counts s-1)
Fe intensity (kilo-counts s-1)
(b5)
R2=0.77
Cr intensity (kilo-counts s-1)
Ca intensity (kilo-counts s-1)
(b6)
R2=0.37
Fe intensity (kilo-counts s-1)
Ca intensity (kilo-counts s-1)

## Figure 3

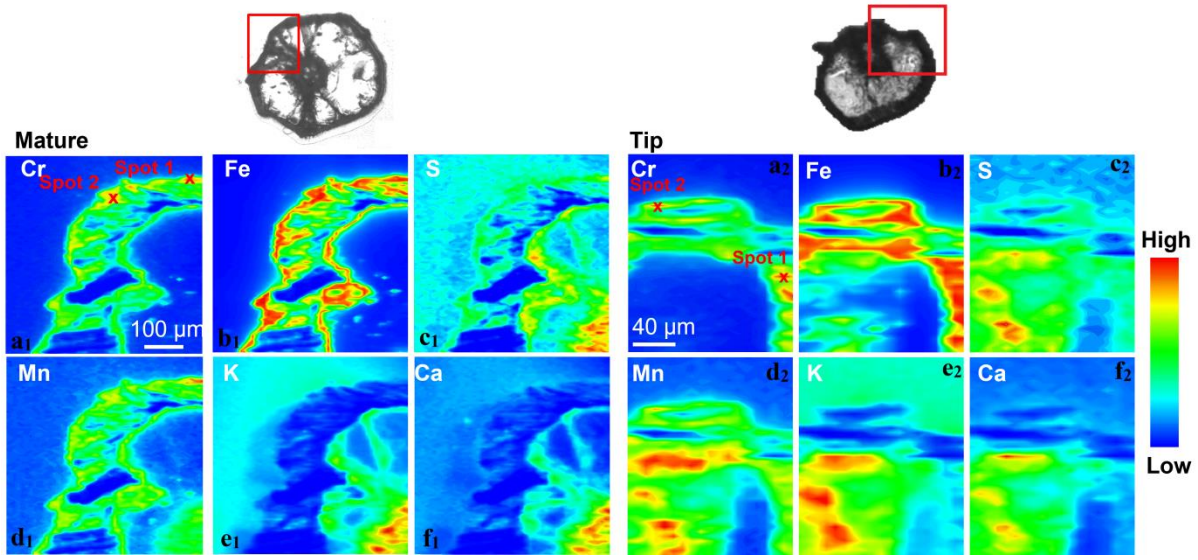

**Figure 4**

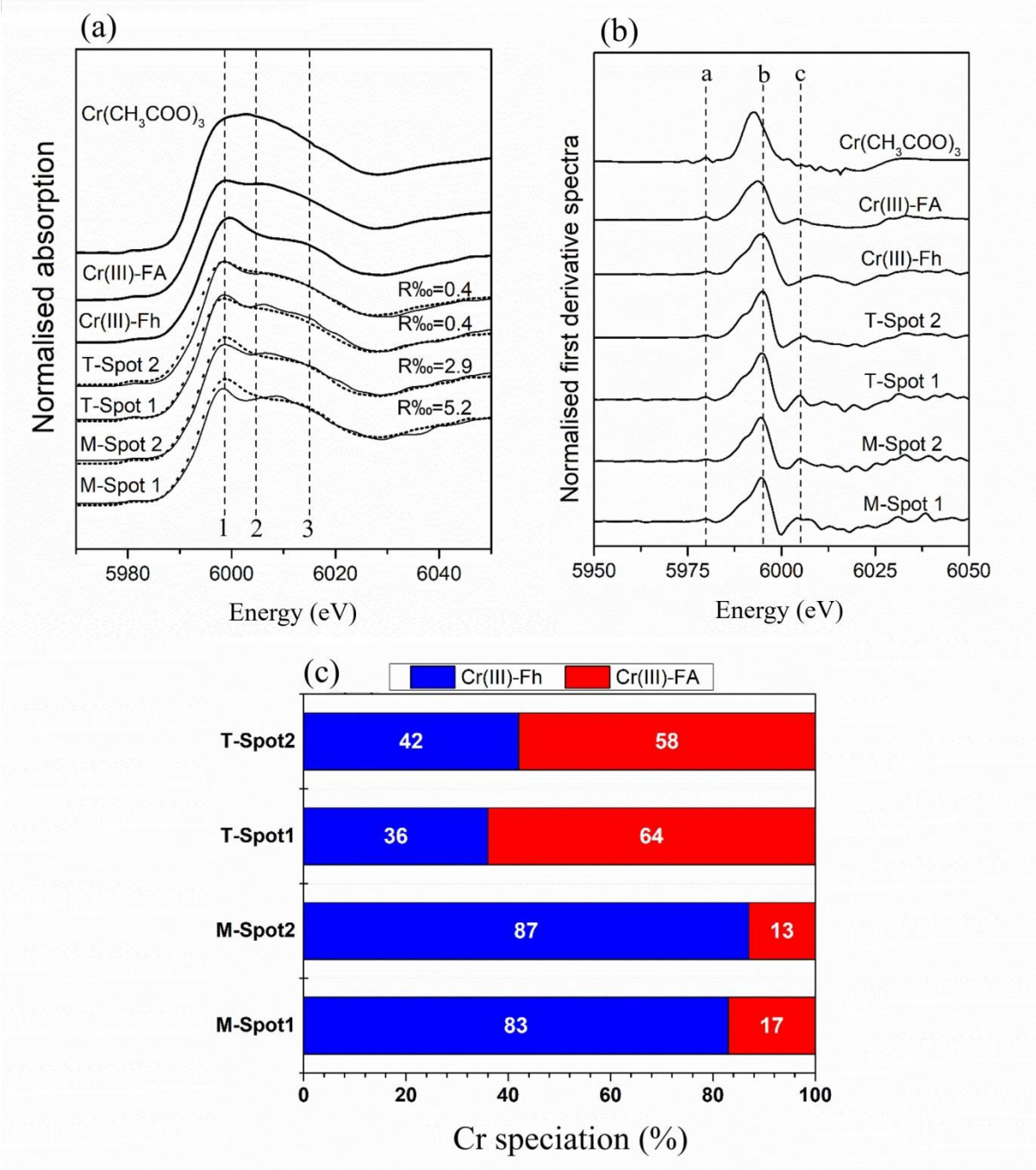
(a)
Normalised absorption
Cr(CH3COO)3
Cr(III)-FA
Cr(III)-Fh
T-Spot 2
T-Spot 1
M-Spot 2
M-Spot 1
R‰=0.4
R‰=0.4
R‰=2.9
R‰=5.2
1
2
3
5980
6000
6020
6040
Energy (eV)
(b)
a
b
c
Normalised first derivative spectra
Cr(CH3COO)3
Cr(III)-FA
Cr(III)-Fh
T-Spot 2
T-Spot 1
M-Spot 2
M-Spot 1
5950
5975
6000
6025
6050
Energy (eV)
(c)
Cr(III)-Fh
Cr(III)-FA
T-Spot2
42
58
T-Spot1
36
64
M-Spot2
87
13
M-Spot1
83
17
0
20
40
60
80
100
Cr speciation (%)

## Figure 5

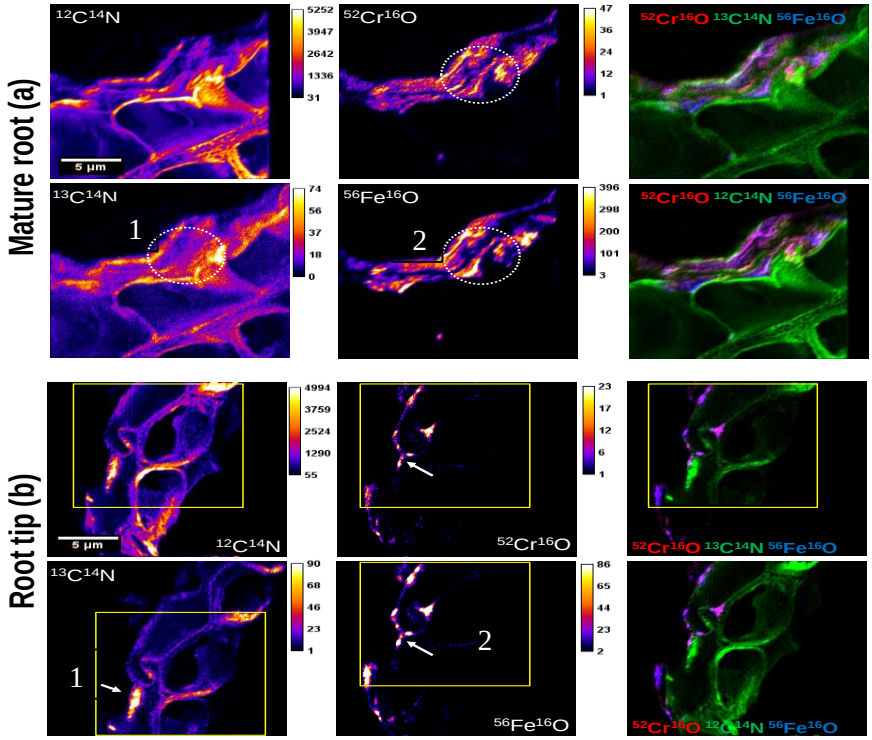
Mature root (a)
Root tip (b)
12C14N
52Cr16O
52Cr16O 13C14N 56Fe16O
13C14N
56Fe16O
52Cr16O 12C14N 56Fe16O
5 µm
1
2
5252
3947
2642
1336
31
47
36
24
12
1
74
56
37
18
0
396
298
200
101
3
4994
3759
2524
1290
55
23
17
12
6
1
90
68
46
23
1
86
65
44
23
2

**Figure 6**

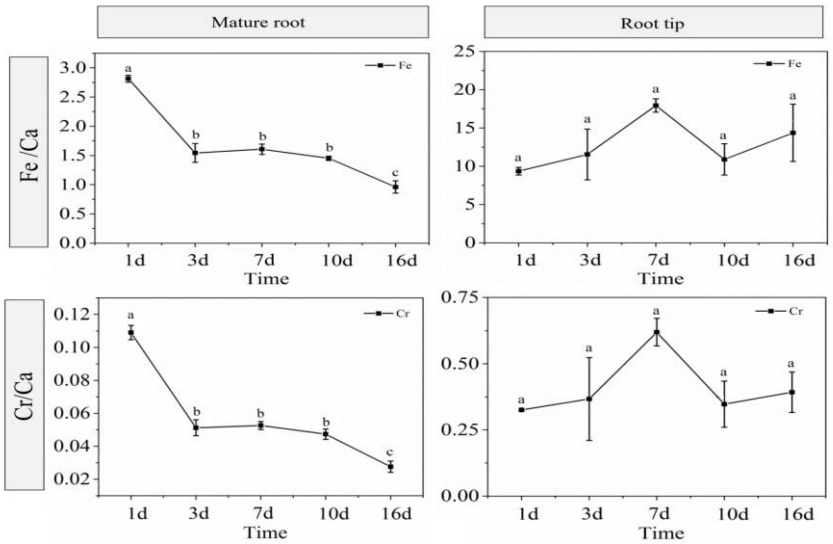

## CRediT authorship contribution statement

[#]XX and PZ equally contributed to this work.

**JY**: designed the experiments. **XX** and **PZ**: performed the lab experiments with the kind guidance of JY. **JY**, **XX** and **PZ**: performed the XRF, XANES and SEM measurements and data analysis. **JY**, **JL**, **RL** and **CR**: conducted the NanoSIMS experiments. **JY**, **JL** and **XX**: performed the NanoSIMS data analysis. **PZ**, XX, **JY** and **JL**: analysed the data and drafted the manuscript. **JY**, **PZ**, **BE**, **ES** and **BBK**: participated in the interpretation of results. **JY**, **CR**, **RL**, **PZ**, **BE**, **ES** and BBK: improved the grammar and corrected spelling mistakes. **PZ**, **JY**, XX, **BE**, **BBK** and **ES**: edited and thoroughly revised the manuscripts. All authors read, corrected and approved the final submitted version of the manuscript.

**Declaration of interests**

■ The authors declare that they have no known competing financial interests or personal relationships that could have appeared to influence the work reported in this paper.

☐The authors declare the following financial interests/personal relationships which may be considered as potential competing interests: